EXPERIMENTS ON THE WALL-PRESSURE HISTORY IN SHOCK REFLECTION PROCESSES

Thesis by

Donald Baganoff

In Partial Fulfillment of the Requirements

For the Degree of

Doctor of Philosophy

California Institute of Technology

Pasadena, California

1964

(Submitted May 14, 1964)

ACKNOWLEDGMENT

The author wishes to express his sincere appreciation to Professor H. W. Liepmann for suggesting the study of the shock reflection process and for his patient guidance and encouragement during the investigation. Discussions with Professors A. Roshko and B. Sturtevant were extremely helpful towards the completion of the present work and are also gratefully acknowledged. Special thanks are due to J. A. Smith who frequently assisted in the operation of the shock tube.

It is a pleasure to thank Mrs. Geraldine Krentler for her competent typing of the manuscript and Mrs. Melenie Loosli for her assistance in the preparation of many of the figures.

The author is indebted to the California Institute of Technology for various forms of financial assistance, and to the National Aeronautics and Space Administration for their fellowship support for two years of study, and for their support of the experiments conducted in the GALCIT 17-in.-diameter low-pressure shock tube.

ABSTRACT

The normal reflection of a plane shock from a plane wall is investigated experimentally using a pressure gauge which has a risetime of 0.1 μsec and no overshoot. Pressure histories of 5 μsec duration can be obtained with this gauge. The experiments were conducted on the end wall of the GALCIT 17-in.-diameter shock tube.

Experimental results for three aspects of the reflection process are discussed: (1) profile for the reflected shock front, (2) effect of a cold wall, and (3) effect of a real gas.

It is concluded that the effect of a cold wall must play a comparatively minor role in the reflection process since the thickness of the recorded profile is comparable to the thickness of the incident shock, and the pressure jump across the profile is about 85 per cent of the ideal value. Also, the pressure history immediately behind the reflected shock can be approximated by boundary layer theory. The effect of a real gas was studied in carbon dioxide and it is shown that the relaxation process behind the incident shock produces a large effect on the recorded pressure history which provides a method of measuring the vibrational relaxation time in carbon dioxide for high temperatures.

TABLE OF CONTENTS

TABLE OF CONTENTS (contd.)

TABLE OF CONTENTS (contd.)

LIST OF FIGURES

LIST OF FIGURES (contd.)

I. INTRODUCTION

The study of the flow through a one-dimensional gas dynamic shock has unquestionably proven to be a rich source of information from both a theoretical and an experimental point of view, especially in the last two decades. In spite of the extensive studies that have been reported over a broad spectrum of problems ranging from high temperature chemistry in the shocked region to studies of the shock front itself, the study of shocked flows will continue to be productive in the future for two important reasons. First, the various phenomena that enter the gas dynamic problem are fundamental in nature and form an almost inexhaustible supply of problems when permuted with the available gases; and, second, new developments in instrumentation continue to expand the practical regions of experimental research and open up new basic areas for investigation.

The subject material of the present work, it is believed, falls in the second category. Since the development of the instrumentation on which the present investigation is based (0.1 μsec risetime pressure gauge) has been reported previously (Ref. 1), the present paper will be restricted primarily to a discussion of the experiment and the resulting conclusions.

The object of the present work is to study, experimentally, the reflection of a plane shock front from a plane wall on a time scale of the order of the mean free time for collisions in the initial gas. The only idealization desired is a one-dimensional flow. Otherwise, the object is to study the effects of using a real gas and a real wall, i.e., heat conducting.

The aspect of this investigation that makes it both new and different from most of the "infinitely denumerable" set of shock reflection studies found in the literature is the time scale of interest. On the time scale of the mean free time for collisions, the physics of such a shock flow (from a gas dynamic point of view) is controlled by heat conduction, viscous dissipation, and (for sufficiently high temperatures) relaxation phenomena such as vibrational relaxation and initial stages of dissociation and/or ionization, depending on the gas. From the kinetic theory point of view, the time scale of interest may be such that a measurable difference would arise between the experimental results and predictions based on the gas dynamic equations of continuum mechanics. Consequently considerable fundamental information on real flows could ultimately be expected from such an investigation.

It is recognized that the problem area, as defined, is quite broad and has to be restricted for manageable

results. Therefore, the present study will be confined to a discussion and analysis of experimental pressure history data (on the wall) for the shock reflection process with the hope that the study will lead to a better understanding of the fundamental processes involved, will point the way to further experimental investigations, and may help in formulating theoretical ideas for similar problems.

The interest in the experimental study of the pressure history on the end wall of a shock tube for the shock reflection process has been guided strongly by the present state of experimental capability. The case of the free running shock profile has been studied extensively by Sherman (Ref. 2) using a hot wire, by Horning and co-workers (Ref. 3 and references cited therein) using an optical technique, by Camac (Ref. 4) using an electron beam, and by Wray and Freeman (Ref. 5) using an ultraviolet absorption technique. However, in each case the experimental method has suffered from one or more limitations such as poor resolution of the shock profile, restricted Mach number range, low pressure, and restriction to a particular test gas. Consequently, with the development of the capability of recording precise pressure history data from the end wall of a shock tube for a time interval of 5 μsec (Ref. 1) and with the demonstrated difficulty of making measurements on the free running shock in mind, it

was decided to investigate the shock reflection process due to its greater flexibility as an experiment (no severe Mach number limitation, most any gas can be used, detailed pressure profile data can be obtained, etc.) even though some aspects of the corresponding theoretical problem are presently extremely difficult.

In order to define the scope of the investigation more clearly, it is advisable at this point to consider what one would expect to observe in the end wall pressure history for the shock reflection process (more accurately, hindsight gained from the experimental results). Figure 1a shows the x-t diagram for the ideal shock reflection and defines the three regions of interest: the initial state ①, the state behind the incident shock ②, and the state behind the reflected shock ⑤. (The numbering order used in reference 6 is being followed here.) If the end wall pressure were recorded on a time scale much larger than the mean free time τ_c in region ① and the gas used were calorically perfect, then one would merely observe a pressure step, equal in magnitude to the Rankine-Hugoniot jump for the reflected shock, as shown in figure 1b. On the other hand, if the gas used were calorically imperfect and observations were made on the same time scale, then one would observe an effect something like that shown in figure 1c due to the re-establishment of the variables of

state after relaxation (this will become clear later). If the time scale for the gas which was assumed to be calorically perfect were reduced to within an order of magnitude of the collision time in region ①, then the effect of the cold wall would appear as a small negative pressure perturbation which would vanish slowly as shown in figure 1d; and on a time scale of the order of the collision time, the reflected shock profile would appear as shown in figure 1e.

Although each effect discussed above is of interest in its own right and could be a subject of individual study, all three effects will be considered here (however separately) because of their close interrelation and the desire to construct a relatively complete picture of the reflection process.

The problem of the normal reflection of a plane shock from a plane heat conducting wall has been treated theoretically by Goldsworthy (Ref. 7) using a boundary layer type of analysis. His solution gives the perturbed trajectory of the reflected shock and the perturbed flow field variables in the reflected region for large time. Experimental verification of Goldsworthy's result for the perturbed trajectory of the reflected shock has been given by Slachmuylders (Ref. 8) and Sturtevant (Ref. 9). The temperature of the wall at the interface between the

wall and the hot gas in the reflected region has been considered by Clarke (Ref. 10), both theoretically and experimentally.

The effect of various relaxation processes on the normal reflection of a plane shock has been treated by a number of investigators, e.g., Spence (Ref. 11) has discussed a linearized theory for the effect of dissociation and vibrational relaxation and suggested that an experimental study of the reflected shock may yield information on relaxation times. Bashenova and Saytzev (Ref. 12) have studied, experimentally, the trajectory of a reflected shock in CO_2.

The reflected shock profile itself has, unfortunately, received little theoretical attention to date.

II. EXPERIMENT

2.1 Shock Tube

The experiment was conducted in the GALCIT 17-in.-diameter low-pressure shock tube. Since the shock tube facility is described in reference 13, only the features that are unique to the present experiment will be discussed.

One of these features is the extremely low leak rate of about 0.01 μHg/hr. (Ref. 13) which made the task of setting and holding the initial pressure in the shock tube to the desired value for the duration of the run a relatively simple matter. This was particularly important for the reflected shock profile studies where the initial pressure was as low as 30 μHg and where it was desired to retain the purity level of the test gas as initially introduced into the driven section of the shock tube.

A second feature is the large diameter of the shock tube which made possible, for the conditions of the experiment, the realization of a comparatively good one-dimensional flow in a small region on the axis of the shock tube where the experiment was conducted. The primary factors which alter the one-dimensional nature of the reflected shock flow, in this region, are the disturbances created by the boundary layer behind the incident shock

and the non-planar surface of the incident shock (shock curvature). Figure 2 presents a scale drawing of a portion of the shock tube at the end wall showing the relative dimensions of the maximum curvature of the incident shock, the maximum thickness of the reflected region, and the pressure gauge. The incident shock shape shown in the figure was reconstructed from the data of reference 14 for an initial pressure of 30 μHg where the curvature of the shock is a maximum for the present experiment. The reflected region shown in the figure was drawn for the condition of maximum reflected shock speed (for the experiment) to show the maximum thickness attained by the reflected region at the end of the experiment (5 μsec). A discussion of the severity of the disturbing influences on the one-dimensional flow of the experiment is presented in appendix A.

The shock Mach number was determined by measuring the transit time of the shock between two thin film heat gauges in the side wall of the shock tube at stations 20 and 70 cm from the end wall. The transit time (ranging from 200 μsec to 1200 μsec for the tests) was recorded on a Berkeley 7260 microsecond counter. The largest source of error in determining the Mach number was the uncertainty of the temperature of the test gas inside the shock tube. Since the shock tube is so massive, its wall temperature

did not always correspond to the room temperature. (Also, on very hot days the driver section was noticeably cooler to the hand than the test section which was above a bank of oscilloscopes and in a stream of hot air produced by the oscilloscopes.) In addition, the free expansion of the test gas into the high vacuum condition of the shock tube ($p_2/p_1 \approx 10^{-3}$) lowered its temperature considerably and it is uncertain how near to thermal equilibrium the test gas came with the wall of the shock tube in the interval before the shock tube was fired. However, it is unlikely that the test gas differed by as much as $12^{\circ}C$ from the room temperature. An estimate for the error introduced into a Mach number computation, due to an uncertainty in the temperature of the gas, can be obtained from the following relation:

$$\frac{dM}{M} = -\frac{1}{2}\frac{dT}{T}$$

For an uncertainty in temperature of $12^{\circ}C$, we have

$$\frac{dM}{M} \approx -\frac{1}{2}\ \frac{12}{300} = -2\%.$$

Therefore one should expect the reported test Mach numbers to be correct to within two per cent.

The initial pressure in the driven section of the shock tube was set by one of two methods. For pressures below 1 mm Hg the test gas was first introduced into a

small vessel which had a volume 10^3 times smaller than the volume of the driven section of the shock tube; there the pressure was measured with a 0 - 50 mm Hg Wallace and Tiernan absolute pressure manometer after which the test gas was dumped into the shock tube. For higher pressures the test gas was introduced directly into the driven section of the shock tube and the pressure was monitored by a 0 - 20 mm Hg Wallace and Tiernan absolute pressure manometer. The largest errors in the initial pressures were probably experienced with the runs at 1 and 5 mm Hg where the Wallace and Tiernan gauge required large corrections to its calibration and where it seemed to exhibit hysteresis effects. At these two pressures the errors could be as large as 5 per cent. A McLeod gauge with a range of zero to one mm Hg (two scales) was used periodically to check the results of the above procedures.

2.2 Arrangement of Equipment

The pressure gauge was located on the centerline of the shock tube to minimize the effect of the shock curvature. A small thin film heat gauge, which was used to trigger the oscilloscopes, was located one inch forward of the end wall and on a radius 6" from the pressure gauge (Fig. 3). The small separation between the end wall and the trigger gauge was necessitated by the practical need

for a small delay time ($\approx$10 μsec), since the data was primarily recorded at an oscilloscope sweep speed of 1 μsec/div; a larger delay time would have made it more difficult to predict the position of the oscillograph trace, due to uncertainties in the shock speed, for each run under new conditions.

Figure 4 presents a block diagram of the triggering circuit and the pressure gauge circuit used in the experiment. Two Tektronix type 555 dual-beam oscilloscopes were used to obtain oscillograph traces of the pressure history for each run. All traces were recorded on 3000 speed Polaroid film with a one to one camera; this gave the largest display of the pressure traces but suffered from the disadvantage that the grid (and consequently the trace itself) was distorted at the edges of the oscillogram. (The distortion was more troublesome because of the resultant curved grid lines than because of the small reduction in grid size at the edges of the oscillogram.)

2.3 Pressure Gauge

One of the key elements in the completion of the present investigation was the pressure gauge used to make the measurements. Here again, since the pressure gauge is described in some detail in reference 1, only the details that are either unique to the present experiment or warrant

repetition will be discussed.

The primary features of the pressure gauge used in the present set of experiments are the extremely short risetime (≈ 0.1 μsec) and the absence of an overshoot or "ringing" in the output signal. However, these features were obtained only at the expense of having a finite time for which the pressure gauge could faithfully reproduce a pressure signal. Figure 5a presents, schematically, the response of the pressure gauge to an applied pressure step and summarizes the important quantities associated with the performance of the pressure gauge. The severe oscillation that sets in limits the useful recording time of the pressure gauge to the duration of the initial flat portion of the response (dwell time).

The dwell time of the pressure gauge is determined by the diameter of the pressure sensing surface of the gauge. Because of shock curvature considerations (see Fig. 2), this diameter was limited to 1 3/8" which resulted in a dwell time of 5 μsec for the gauge. Figure 5b shows the response of the gauge to the pressure step produced by a reflected shock for which the incident Mach number was $M_s = 1.19$ and the driven gas was air at a pressure of one atmosphere. In addition to the quoted risetime and dwell time, the figure shows a slight decay in the signal of about 2 per cent. This decay is a result

of the electrical circuit which was used in conjunction with the pressure gauge.

Details of the pressure gauge circuit and supporting equipment are discussed in appendix B.

2.4 Pressure Gauge Calibration

Although the pressure sensitivity of the basic gauge is quite reproducible from gauge to gauge, the size of the capacitor that forms the sensing element is generally so small (≈ 100 $\mu\mu$f) that parasitic capacitance in the gauge circuit (coaxial cables, etc.) changes the apparent sensitivity of the gauge and requires that a calibration be made of a particular gauge and gauge circuit combination for accurate analysis of data.

Figure 6 presents the calibration of the gauge. The jump in voltage was measured from a number of traces and plotted against the theoretical pressure jump for a known incident shock Mach number and initial pressure. The voltage jumps plotted in figure 6 are the voltages appearing across the 1.8 MΩ grid resistor R_1 (without the 30 DB amplification, see appendix B) and normalized to a common gauge voltage of 1 kV. The sensitivity of the gauge as read from the figure is 18.5 μv/mm Hg at 1 kV. Most of the data points for the calibration seem to fall within a 5 per cent spread. This spread is not unexpected in view

of the previously discussed uncertainty in the determination of the Mach number and the initial pressure which would affect the abscissa of the plotted points.

2.5 Test Gases

The effect of a cold wall on the pressure history behind a reflected shock was studied in argon and nitrogen. Carbon dioxide was used to study the effect of vibrational relaxation on the pressure history behind a reflected shock, and all three gases were used to study the reflected shock profile. The gases used were taken directly from commercial cylinders without any attempt at further purification.

III. EXPERIMENTAL RESULTS

Although the reflected shock profile data was collected first during the course of the experimental investigation and probably accounted for a major portion of the experimental effort, the large time-scale studies of the effect of a cold wall and the effect of vibrational relaxation on the shock reflection process will be considered first because of their usefulness in setting the stage for interpreting the profile data.

3.1 Effect of a Cold Wall on the Pressure History Behind a Reflected Shock

3.1.1 Experimental results for argon and nitrogen.

Figures 7 and 8 present a series of pressure traces for reflected shocks in argon and nitrogen showing the effect on the pressure due to heat transfer to the cold end wall. Similar runs were made in the two gases for the same initial pressures. The resultant Mach numbers are not exactly the same but are close enough for visual comparison of the traces between the two gases because the Mach number dependence, as will be seen, is rather weak. All of the traces run from right to left; the upper traces were recorded at a sweep speed of 1 μsec/div and the lower traces at 5 μsec/div. The lower trace was used to

determine whether or not the pressure profile had to be corrected for a slope in the "zero line" (see Fig. 7b). For detailed analysis additional oscillograms were obtained using an oscilloscope sweep speed of 1/2 μsec/div. These were obtained with a second oscilloscope simultaneously with the recording of the pressure traces shown in the figures.

A horizontal line was drawn above the upper trace of several of the oscillograms (the ones for which there was very little slope in the zero line) to indicate the asymptotic limit for the pressure (its determination will be explained below) and to show more clearly the behavior of the pressure perturbation due to the heat transfer to the cold end wall of the shock tube. It is evident from an inspection of the pressure traces that the pressure perturbation is a small fraction of the total pressure jump and extends over a time scale much greater than the time scale for the reflected shock profile. Also a comparison of similar runs for argon and nitrogen shows that the effect of heat transfer is spread out over a longer time scale in argon than for nitrogen, indicating a dependence on the value of the thermal conductivity and the gas constant.

It is noteworthy that the initial pressure must be around 1 mm Hg to observe the major effect of heat transfer

within 5 μsec. This comparatively high pressure (due to the 5 μsec limitation of the pressure gauge) rules out a thorough study of the effect of heat transfer in rare gases in a large shock tube.

3.1.2 Discussion of two perturbation theories for the heat transfer effect. The problem of the normal reflection of a plane shock from a plane heat conducting wall has been treated by Goldsworthy (Ref. 7). Goldsworthy's solution is the result of a boundary layer type of analysis and is therefore limited to large time. (What is meant by large time for the case of the pressure perturbation on the end wall will be discussed later with respect to the experimental results.) The analysis divides the region behind the reflected shock into two parts: a boundary layer near the wall in which heat conduction plays a dominant role, and a region of inviscid linearized flow between the reflected shock and the boundary layer. The principal assumptions made in the analysis are that the thermal conductivity of the gas varies linearly with the temperature, and the quantities in the inviscid flow and the jump conditions on the reflected shock are perturbed only slightly from the ideal values.

The theoretical pressure perturbation on the end wall is given by equation 55 of Goldsworthy's paper and

can be written in the following dimensionless form:

$$\frac{p'}{p_5} = - B(M_s)\ (1 - T_1/T_5)\ \frac{1}{\sqrt{\tilde{t}}} \quad , \qquad (1)$$

where

$$\tilde{t} = t/\tau_5$$

$$\tau_5 = \frac{\gamma^2}{\pi}\ \frac{k_5}{c_p \rho_5\ a^2_5} = \frac{\gamma^2}{\pi P_r}\ \frac{\mu_5}{\rho_5 a^2_5} \quad ,$$

T_1 is the temperature of the end wall, the quantities with the subscript 5 are the ideal values in region ⑤ (for a thermally insulated wall), and $B(M_s)$ is a weak function of the incident Mach number M_s and the gas constant γ . The function $B(M_s)$ is plotted in figure 9 for two values of the gas constant corresponding to argon and nitrogen. (Two sign errors were found in equation 55 of reference 7 which were corrected in plotting the function $B(M_s)$ in figure 9.)

The characteristic time τ_5 has been expressed in terms of viscosity because viscosity data is generally more readily available for gases at elevated temperature.

The characteristic time τ_5 can be shown to be roughly equal to the collision time τ_{c5} in region ⑤ . Since the ratio of the mean speed $\bar{c}$ to the speed of sound a is

$$(\bar{c}/a)^2 = 8/\pi\gamma \quad ,$$

and since

$$\mu = \varkappa \rho \bar{c} \lambda \qquad (\tfrac{1}{3} < \varkappa < \tfrac{1}{2})$$

then

$$\tau_5 / \tau_{c5} = 8\gamma\varkappa / \pi^2 \, P_r .$$

For $\varkappa = 1/2$, $P_r = 2/3$, and $\gamma = 5/3$, we have

$$\tau_5 / \tau_{c5} = 10/\pi^2 \approx 1.$$

Before comparing equation 1 to the experimental results, it is interesting to consider another problem which can be considered to be a crude approximation of the experiment. The problem is the linearized treatment of the sudden contact between a hot gas and a cold wall. In this case one has to assume that the wall temperature is only slightly less than the gas temperature, i.e.,

$$(T_5 - T_1)/T_5 \ll 1,$$

and the Prandtl number is equal to 3/4. The solution to this problem has been given by Clarke (Ref. 15) and Kubota (Ref. 16). The pressure perturbation at the wall can again be written in the following form:

$$\frac{p'}{p_5} = - (1 - T_1/T_5) \frac{1}{\sqrt{\tilde{t}}} \qquad (2)$$

where in this case τ_5 is evaluated for $P_r = 3/4$.

The striking agreement between equations 1 and 2 is due to the fact that perturbations from the boundary layer affect the strength of the reflected shock but the reverse coupling between the shock and the boundary layer is not nearly so strong. This is precisely the reason why the coefficient $B(M_s)$ in equation 1 is so nearly equal to one; this can be verified by tracing the contribution to the solution from the shock boundary condition in Goldsworthy's analysis.

3.1.3 Comparison of theory and experiment.

Although the pressure traces in figures 7 and 8 look as though the perturbation pressure behaves like $1/\sqrt{t}$, they are by no means refined enough to test the law directly since it would require a comparison of small differences. However, in terms of the dimensionless time $\tilde{t}$ and a suitable non-dimensional ordinate, one should be able to conclude from a plot of the experimental data what is meant by "large time" for the boundary layer analysis, what is a representative time scale for the heat transfer effect on the end wall pressure, the extent to which the heat transfer depresses the pressure jump across the reflected shock, and whether or not the characteristic time τ_5 is the proper time scale for different gases,

pressures, and Mach numbers.

Since a 5 per cent difference in pressure is certainly small enough to be considered a small perturbation and is still large enough to be observed on an oscillogram, the time corresponding to a theoretical 5 per cent perturbation will be used for comparison with the experimental data and as a measure of a characteristic time for the heat transfer effect. The dimensionless time corresponding to a 5 per cent perturbation in the pressure is roughly 400 if one neglects the small correction introduced by the factor $B(M_s)\ (1 - T_1/T_5)$ in equation 1. Therefore the pressure perturbation, according to theory, is less than 10 per cent after roughly 100 collisions in the reflected region and less than 5 per cent after roughly 400 collisions.

The viscosity data of Amdur and Mason (Ref. 17) was used to compute the characteristic time τ_5 for both argon and nitrogen as a function of the incident Mach number. A far more convenient expression for plotting can be obtained from the characteristic time τ_5 as follows:

$$\tau_5 = \frac{\gamma^2}{\pi P_r} \frac{\mu_5}{\rho_5 a_5^2} = \frac{\gamma}{\pi P_r} \frac{\mu_5}{P_5} ,$$

or

$$p_1 \tau_5 = \frac{\gamma}{\pi P_r} \frac{\mu_5}{(p_5/p_1)} \quad . \tag{3}$$

Figure 10 presents a plot of $p_1 \tau_5$ versus incident Mach number for the two gases. Equation 1 was then used to compute the dimensionless time at which a 5 per cent perturbation would occur in the pressure, i.e.,

$$\tilde{t}_{5\%} = 400 \left[B(M_s) \left(1 - T_1/T_5\right) \right]^2 .$$

The physical time at which a 5 per cent perturbation in the pressure occurs is then

$$t_{5\%} = \tau_5 \tilde{t}_{5\%}$$

or, for plotting purposes,

$$p_1 t_{5\%} = (p_1 \tau_5) \tilde{t}_{5\%} .$$

The quantity $p_1 t_{5\%}$ is presented in figure 11 as a function of Mach number for argon and nitrogen. The figure shows a difference in $t_{5\%}$ of roughly a factor of four between argon and nitrogen, for identical conditions, which certainly should be observable in the experimental data.

The location of the theoretical 5 per cent is shown in each of the oscillograms of figures 7 and 8 by a small

triangle. (The time origin was arbitrarily placed at the intersection point determined by a line drawn through the maximum slope of the reflected shock profile and the "zero line".) The reason for the difference between the trace for argon and the trace for nitrogen at, say, 1 mm Hg becomes apparent. For identical conditions the time to the 5 per cent point is some four times greater in argon than in nitrogen which shows up as an apparent larger pressure perturbation in argon. Comparisons between, say, figures 7a and 7c (variation in M_s) and between, say, figures 7a and 8a (variation in μ and ν) show that the boundary layer theory is in qualitative agreement with the experimental results.

There is little doubt that Goldsworthy's boundary layer theory is correct for large times (see Ref. 9) and that it should fail to hold near the shock; but the range of validity can only be decided by experimental data (or an exact theory if it were available). Therefore, if we assume the large time behavior is adequately predicted by equation 1, then it is quite meaningful to plot the pressure profile data in non-dimensional form to determine the behavior in the intermediate range. Figure 12 presents the pressure data from several oscillograms in non-dimensional form. The time axis was non-dimensionalized by the theoretical time $t_{5\%}$ and the pressure axis by the ordinate

at $t = t_{5\%}$. Use of the ordinate at $t = t_{5\%}$ was necessary because the traces do not extend far enough to give the pressure jump at "infinity" and is justifiable on the grounds that we are looking for gross effects. Most of the data was taken from the argon traces because the pressure perturbation in nitrogen was far too small to record and plot in the figure without introducing unacceptable errors. (It should be noted that the data was taken from oscillograms for which the sweep rate was 1/2 μsec/div.)

The conclusions from an inspection of figure 12 are quite striking. On a gross scale one can conclude that the scaling with τ_5 must be correct since there are no severe departures between the different experimental curves and from the curve for the boundary layer theory. One would certainly expect the curves to depart near their respective shock profiles because one could not expect the shock profiles to scale with the heat transfer time scale τ_5. However, the curves are close enough to conclude that, in general, the effect of the heat transfer to the cold wall depresses the pressure jump across a reflected shock to about 85 to 90 per cent of the value for a thermally insulated end wall. This is quite significant in trying to determine the magnitude of the effect of the heat transfer on the reflected shock profile and the extent of

the coupling between the two problems. Also, from the point of view of a pressure jump, the boundary layer theory gives a surprisingly good value for the pressure perturbation on the end wall for times as short as one or two "shock thicknesses". As a final comment it should be noted that the boundary layer theory gives an acceptable value for the dimensionless pressure perturbation on the end wall for $p'/p_5 \leq .10$ or for $t \geq 100 \ \tau_{c5}$ (collision time based on the reflected region).

3.2 Effect of Vibrational Relaxation on the Pressure History Behind a Reflected Shock

Carbon dioxide was primarily chosen as a representative gas for studying the effect of vibrational relaxation on the end wall pressure history for the shock reflection process because of its relatively low characteristic vibrational temperatures which cause a significant effect for moderate Mach numbers. Also, because of the reflected shock profile studies conducted with CO_2 (reported in the next section), it was found desirable to study the "large time" behavior of the shock reflection process in CO_2 in order to help clarify the picture for the reflected shock profile.

3.2.1 Experimental results for CO_2. Figure 13 presents some typical pressure traces for the runs in

CO_2. Again, the time axis runs from right to left and the upper trace, in each case, was recorded at an oscilloscope sweep speed of 1 μsec/div. The indicated Mach numbers are frozen Mach numbers and are based on a sound speed corresponding to $\gamma = 7/5$, i.e., $a = .280$ mm/μsec at 300° K. (This selection is naturally arbitrary and was chosen because of simplifications introduced into the computations for the pressure jumps given below.) Due to the comparatively high initial pressures, the thicknesses of the reflected shock profiles are less than the resolution time of the pressure gauge, except for possibly the run at 500 μHg, and will be treated here as discontinuities. The traces in the figures (except for figure 13d) show an initial "discontinuous" pressure jump and then a relaxation to "equilibrium". It seems quite obvious that the initial jump must be due to frozen conditions in the gas but the nature of the equilibrium state has to be clarified. It should be noted that since the relaxation phenomena produces such a large effect in CO_2, any "corrections" due to the heat transfer effect considered in the last section can be ignored for all practical purposes.

3.2.2 Pressure jump calculations. In order to determine which relaxation processes are taking place and in what regions of the flow, some computations have to be made for the purposes of comparison.

An x-t diagram for a reflected shock in a relaxing gas shows that there are two relaxation regions: one behind the incident shock, and one behind the reflected shock. Since the extent of the relaxed region in ② is greater than the extent of the relaxed region in ⑤, because of the lower temperature and pressure, there are conceivably three combinations of jumps between states. This is shown schematically in the following sketch where F stands for frozen and E stands for equilibrium. (A discussion of the shape of the reflected shock trajectory in a relaxing gas can be found in reference 11.) If we assume that the relaxation time in region ② is much longer than in region ⑤, then we should expect to see three distinct pressure levels in the end wall pressure history corresponding to the jumps F ② - F ⑤, F ② - E ⑤, and E ② - E ⑤, and in the corresponding order. The problem before us is to determine which jumps are observed in the experimental pressure traces and the nature of the equilibrium state reached by the gas.

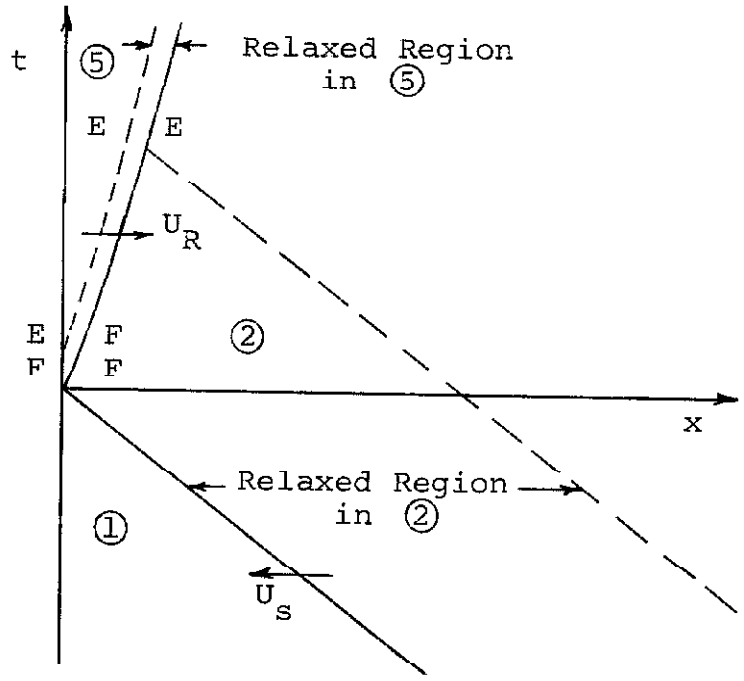

The equations used in computing the above pressure jumps for the present analysis are summarized in appendix C. It suffices here to remark that the method is an iteration method whereby the density jump is guessed first and the pressure and enthalpy jumps are then computed; the second approximation to the density jump is then obtained from a Mollier diagram (this procedure is discussed in reference 6). For the case of vibrational relaxation, the perfect gas relation with a fixed gas constant remains valid and the Mollier diagram can be replaced by a curve

of enthalpy versus temperature.

Figure 14 presents a plot of non-dimensional enthalpy h/RT_1 versus the temperature ratio T/T_1 for CO_2 ($T_1 = 300^\circ$ K). The vibrational contribution to the enthalpy, $(h/RT_1)_{vib}$, was computed from the well-known relation obtained from quantum statistical mechanics

$$(h/RT_1)_{vib} = \left[\sum_{i=1}^{n} \frac{z_i}{e^{z_i} - 1}\right] \left(\frac{T}{T_1}\right) , \qquad (4)$$

$$z_i = \theta_{vi}/T .$$

The four characteristic vibrational temperatures θ_{vi} were computed from data given by Bethe and Teller (Ref. 18). The frequencies of the four normal modes of vibration of the CO_2 molecule (obtained from spectroscopic data), as quoted by Bethe and Teller, are

$$\nu_i = 667,\ 667,\ 1336, \text{ and } 2350 \text{ cm}^{-1}$$

(units in waves/cm). The characteristic temperatures θ_{vi} were then computed from the relation

$$\theta_{vi} = \left(\frac{hc}{k}\right) \nu_i = 1.440 \ \nu_i \ (^\circ\text{K}),$$

where h, c, and k are the familiar universal constants. The lowest characteristic temperature corresponds to the

temperature ratio $T/T_1 = 3.20$ and the highest corresponds to the temperature ratio $T/T_1 = 11.3$. It is apparent from figure 14 that the vibrational energy must be in error at the larger temperature ratios because of the onset of anharmonic vibration and the breakdown of the harmonic oscillator model used to obtain the simple expression given by equation 4. However, on a first attempt at fixing ideas on the shock reflection process one can afford to be somewhat cavalier with finer details. The dissociation curves drawn in the figure (dashed lines) were interpolated from the data given by Raymond (Ref. 19) and may be quite rough since his computed points were spaced for an enthalpy-temperature diagram extending to a much higher temperature. The dissociation curves were drawn to give an idea of what the temperature in the reflected region would be if the gas reached complete thermal equilibrium. In the following, "equilibrium" (E)will mean vibrational equilibrium as given by the upper solid curve in figure 14 and "frozen" (F) will mean the enthalpy given by a straight line of slope 7/2 passing through the equilibrium curve at the point $T/T_1 = 1$.

Figures 15 through 17 present the results of the computations for the pressure, temperature, and density jumps respectively across the incident and reflected shocks for the various jumps between the two thermodynamic states of the gas. The symbol F ② - E ⑤, for example, means a

jump from a frozen state in region ② to an equilibrium state in region ⑤.

3.2.3 Comparison with experimental results. The experimental pressure traces were used to measure two pressure jumps (with the aid of the gauge calibration curve given in figure 6) which are shown plotted in figure 15; the initial discontinuous pressure jumps are plotted as circles and the equilibrium pressure jumps are plotted as triangles. It should be noted that the equilibrium point was not reached, within the 5 μsec limitation of the pressure gauge, for the run at the lowest Mach number (due to the low temperature) and for the two highest Mach number runs (due to the low initial pressure required by the shock tube). An inspection of the distribution of circles indicates that the initial jump is the frozen-frozen jump as one would expect. An inspection of the distribution of triangles indicates that the plateaus in the pressure traces correspond to vibrational equilibrium in both region ② and region ⑤.

One of the striking features of the experiment is the extreme sensitivity of the reflected pressure to the conditions in region ②. In going from the condition $F_{②} - E_{⑤}$ to the condition $E_{②} - E_{⑤}$, the reflected pressure changes by a factor of two for the Mach number

$M_s = 7$; this is quite significant for determining which processes are taking place in region ②. However, it is unfortunate in the sense that region ② is the region of lower temperature and is consequently less interesting than region ⑤.

The present results indicate that all vibrational modes of the CO_2 molecule are fully excited in region ② within the relaxation time determined by the pressure traces. This is in agreement with the data presented by Zienkiewicz and co-workers (Ref. 20) and is in disagreement with the data of figure 6.7 of the article by Griffith in reference 21 where it is concluded that only the two lowest vibrational modes are fully excited, within the measured relaxation time, for Mach numbers up to $M_s = 7$. This item could certainly be pursued in more detail with the present experimental method and would be an interesting problem for future investigation.

Some further interesting observations can be made from an inspection of the pressure traces and the curves of figure 15. If the relaxation time in ② were much longer than the relaxation time in ⑤, then the theoretical curves of figure 15 would indicate that the end wall pressure history should be somewhat as shown in the following sketch.

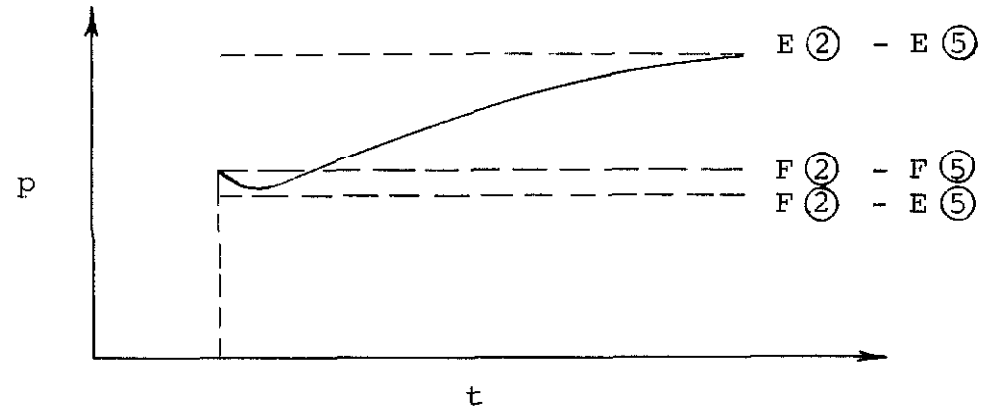

The sketch shows that a relaxation process in ⑤ depresses the pressure and a relaxation process in ② raises the pressure (a good diagnostic tool). Since the above behavior is not observed in any of the experimental pressure traces (even for the low Mach number case of figure 13d), it must be concluded that the relaxation region behind the incident shock can not be much greater in extent than that behind the reflected shock. This can be argued as follows. If we assume that the experimental trace is, roughly, a sum of two relaxation processes of simple exponential character, then the initial slope depends on the ratio of the two "relaxation" times and the ratio of the pressure difference as shown below.

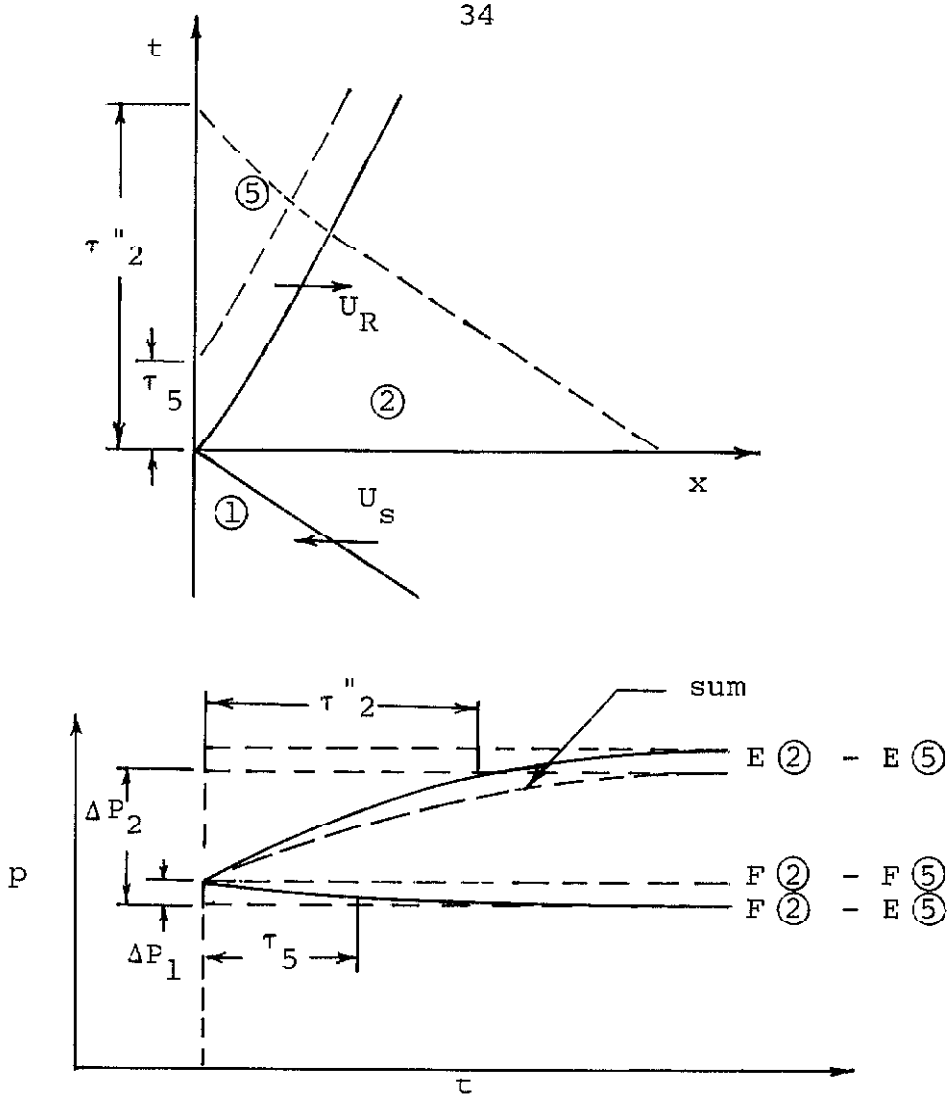

Therefore a positive initial slope indicates that the following relationship must exist:

$$\tau''_2/\tau_5 \quad < \Delta P_2/\Delta P_1 \ .$$

For $M_s = 7$, figure 15 gives

$$\tau''_2/\tau_5 \quad < \frac{721 - 354}{412 - 354}$$

or

$$\tau''_2/\tau_5 \quad < \quad 6.3.$$

Since the initial slopes on the pressure traces are far from being zero, the ratio is probably much closer to one than to six. The above ratio should only be used in forming a mental picture of the flow field and should not be used for quantitative statements concerning relaxation times in the two regions. However, with this mental picture one can now investigate the relaxation time in region ② in more detail.

3.2.4 Vibrational relaxation time in CO_2. The relaxation times indicated by the pressure traces are therefore primarily a measure of the relaxation time in region ② and shed no light on the relaxation time in region ⑤. (This may not be true for other gases.) In order to use the experimental data for quantitative statements on the relaxation time behind the incident shock τ_2, a relationship has to be found relating the relaxation time of the pressure traces τ'_2 to the actual relaxation time τ_2.

The appropriate geometrical relationships and the necessary approximations needed in the calculations of the ratio τ_2/τ'_2 are presented in appendix D. The computed

ratio τ_2/τ'_2 is presented in figure 18 as a function of incident Mach number. Figure 18 shows that the ratio of the actual relaxation time in region ② to the relaxation time observed in the oscillograms is on the order of five.

The quantity τ'_2 was determined from an oscillograph trace by assuming the standard 1/e type definition, i.e., the point where the relaxation part of the trace decayed to 1/e of its initial value at the shock. (This can not be taken too seriously because some pressure traces, e.g., figure 13a, do not resemble an exponential type relaxation as closely as others; the low Mach number runs in general look better than the high Mach number runs in this respect.) The resulting relaxation times τ_2 are presented in figure 19 along with the data obtained by Blackman (Ref. 22) using an interferometer. The present data was plotted using an elongated "H" symbol to display the full range in temperature and pressure in region ② between the frozen conditions immediately behind the shock and the equilibrium conditions downstream from the incident shock. Blackman, however, plots only average values which is a little misleading.

Some general conclusions which can be drawn from figure 19 are as follows:

(1) The relaxation times in region ②, as determined by the present experiment, are consistent with

previous measurements reported for CO_2.

(2) The observed behavior of the pressure traces can be identified with a relaxation process in region ②.

(3) The present experiment gives a method for measuring the vibrational relaxation time in region ② for higher temperatures and lower pressures than can be obtained with an interferometer.

The use of a shock wave for the experimental determination of the vibrational relaxation time in a gas must, for purposes of simplicity, be restricted to the Mach number range (or temperature range in region ②) for which the relaxation length behind the shock is at least ten times the thickness of the shock front. Hence, a maximum Mach number exists, for each gas, above which it becomes impractical to use shock waves for the experimental determination of relaxation time. (This is due to the fact that both the shock front thickness and the vibrational relaxation length scale, to a first approximation, inversely with pressure.) For CO_2 the maximum Mach number is $M_s \approx 8$ ($1/\sqrt[3]{T} \approx .07$). Figure 19 shows that the range of temperatures between the abscissa $1/\sqrt[3]{T} \approx .07$ and the data obtained by Blackman using an interferometer is covered by the present experimental method. An oscillogram showing the relative time scales between the part of the trace due to vibrational relaxation and the part due to the reflected

shock profile, for M_s near the maximum value for CO_2, is presented in one of the figures of the next section, figure 22d.

For gases possessing longer relaxation times, the corresponding maximum Mach numbers (or temperatures) are greater. Some rough estimates for O_2 and N_2 (using extrapolated data and ignoring dissociation and ionization) are as follows: $M_s \approx 12$ for O_2 and $M_s \approx 18$ for N_2. For both gases the initial pressures would have to be around 100 μHg so that the duration of the relaxation process would be greater than the risetime of the pressure gauge. Due to the 5 μsec limitation of the pressure gauge, the initial pressures would have to be rather high for studies in O_2 and N_2 at lower Mach numbers. For $M_s \approx 8$ the initial pressure would have to be around 10 mm Hg for O_2 and around 100 mm Hg for N_2. (Redesign of the pressure gauge could increase the dwell time by a factor of three or four which would decrease the required initial pressure by the same factor, see reference 1.) Since the above test conditions are considerably beyond the performance range of the GALCIT 17-in.-diameter shock tube, no attempt was made to investigate vibrational relaxation in O_2 and N_2.

3.3 Reflected Shock Profile

A comprehensive discussion of the experimental results for the reflected shock profile is impeded by the extreme difficulty of the corresponding theoretical problem and the resulting scarcity of suitable methods for computing a theoretical reflected shock profile. (This is due to the fact that the flow is basically nonsteady and can not be reduced to a steady flow by a transformation of coordinates, and hence always depends on the two coordinates x and t.) Nevertheless, some definite general observations can be made with regard to the experimental data which it is felt are of importance in understanding the physics of the reflection process, in aiding future theoretical efforts, and in identifying potentially productive areas for further experimental research.

3.3.1 Experimental results for A, N_2, and CO_2.

Some examples of profiles for reflected shocks are presented in figures 20 through 22 for argon, nitrogen, and carbon dioxide. As before, the time axis runs from right to left. The upper trace was recorded at a sweep speed of 1 μsec/div and the lower trace at 5 μsec/div. The noise level in some of the oscillograms is noticeably higher than in many of the above traces because of the greater sensitivities required for the reflected shock profile studies (due to

the lower initial pressures and the resulting lower pressure jumps). It is of interest to note that a typical initial pressure in the shock tube must be around 100 μHg for studies of reflected shock profiles on a microsecond time scale, whereas the heat transfer studies discussed above were conducted at an initial pressure of around 1 mm Hg (a factor of ten in the characteristic time scale).

Only examples for comparatively high Mach numbers are presented in the figures for argon and nitrogen since a rough idea can be obtained from figures 7d and 8d for $M_s \approx 3$. For the case of CO_2 it was necessary to hold the incident Mach number as low as possible in order to minimize the effect of vibrational relaxation. An example of the effect of vibrational relaxation on the profile within and immediately behind the shock front is given in figure 22d. The Mach numbers given in the figures for the CO_2 data are, again, frozen Mach numbers based on $\gamma = 7/5$.

A comparison of pressure profiles points out the very interesting result that the shapes of the reflected shock profiles are roughly the same and independent of Mach number and type of gas used (monatomic or polyatomic). Also, the overall thickness is very nearly the same for all three gases for similar conditions.

3.3.2 Rotational relaxation in N_2 and CO_2. The frozen-frozen pressure jump considered in the last section for CO_2 was computed for $\gamma = 7/5$ (assuming full translational and rotational excitation) and was found to agree rather well with the experimental data. However, in considering the details of the shock profile itself, one might question whether or not a substructure exists where full rotational excitation of the molecule takes place only after completion of translational excitation. If one assumes the translational relaxation time is much shorter than the rotational relaxation time, then one would also expect to see a profile with two distinct pressure levels corresponding to $\gamma = 5/3$ and $\gamma = 7/5$. Here again, one can compare theoretical pressure jumps for $\gamma = 5/3$ and $\gamma = 7/5$ against the experimental profiles in order to identify the structure of the reflected shock profile.

Figure 23 presents two separate plots. The upper pair of curves give the pressure jumps p_5/p_1 for $\gamma = 5/3$ and $\gamma = 7/5$ as a function of incident Mach number, and the lower curve gives the ratio of the pressure jump for $\gamma = 5/3$ to the pressure jump for $\gamma = 7/5$ (for a fixed shock speed), i.e.,

$$P_\gamma = \left. \frac{(p_5/p_1)_{\gamma = 5/3}}{(p_5/p_1)_{\gamma = 7/5}} \right|_{U_s = \text{const.}}$$

The ratio P_γ was plotted against the Mach number corresponding to $\gamma = 7/5$ in order that direct comparisons could be made with the Mach numbers reported with the experimental data. The ratio is very nearly equal to $P_\gamma = 0.7$ for all values of incident Mach number. The reason for the reduction in pressure can be seen as follows. If we assume an incident shock Mach number (based on $\gamma = 7/5$) of $M_s = 9$, then the pressure ratio is given by the point marked A in the figure. If the initial jump is due to translational relaxation only ($\gamma = 5/3$), then, for the same shock speed, the appropriate shock Mach number becomes

$$M_s \ (\gamma = 5/3) = \sqrt{\frac{7/5}{5/3}} \ M_s \ (\gamma = 7/5)$$

$$= .9166 \ M_s \ (\gamma = 7/5) \ .$$

The pressure ratio is then given by the point marked B on the curve for $\gamma = 5/3$ in the figure.

The fractional difference in the two pressure ratios from an experimental point of view, is quite large. Therefore, if an appreciable lag occurred in the rotational relaxation of either N_2 or CO_2, one could expect a significant departure between the pressure jump across the reflected shock profile and the theoretical jump for $\gamma = 7/5$.

The pressure levels corresponding to the two jumps

are indicated on each oscillogram of figures 21 and 22. The marks were located by using the pressure ratios given in figure 23 and the gauge calibration. No attempt was made to compensate for the cold end wall. Therefore the marks should be about 10 per cent high in each case. Since the separation between the two pressure jumps is much greater than the small uncertainty in the experimental data, one can conclude quite definitely from an inspection of the N_2 and CO_2 profiles that a major portion of the rotational relaxation must take place within the shock profile for both gases.

3.3.3 Reflected shock thickness. For a highly viscous flow such as the normal reflection of a shock front, the normal stress experienced by a pressure gauge does not correspond to the thermodynamic pressure p but to the normal component of the stress tensor P_{xx}, i.e.,

$$P_{xx} = - p + \tau_{xx} ,$$

which for one-dimensional flow reduces to

$$P_{xx} = - p + \tau .$$

Therefore the profiles presented in figures 20 through 22 are profiles of P_{xx} rather than profiles of the thermodynamic pressure p. However, on both sides of the profile the viscous stress τ approaches zero quite rapidly

and the stress tensor P_{xx} and the thermodynamic pressure p become equal. Therefore, behind the shock front, the profile can be compared directly to the thermodynamic pressure as was done above.

The present discussion will be restricted to the usual gross description of shock profiles, i.e., the reflected shock profile will be described by its maximum slope thickness and how it varies with incident Mach number and gas properties.

A comparison of figures 20a and 20c, where the initial pressure has been doubled and the incident Mach number held roughly constant, shows that the reflected shock thickness is roughly proportional to the mean free path length λ_1 in region ①. A comparison of figures 7d and 20d, where the initial pressure has been reduced by a factor of two and the incident Mach number has been doubled, shows that the reflected shock thickness is, roughly, inversely proportional to the incident shock velocity, i.e., the behavior is the same as that observed by a stationary observer viewing a free running shock.

Using the above clues, an effective reflected shock thickness δ_r can be defined by

$$\delta_r = \Delta t_r U_s,$$

where Δt_r is the maximum slope thickness of the pressure-time trace as read from the oscillogram, and U_s is the incident shock velocity. One can then form the dimensionless ratio

$$\lambda_1/\delta_r = \lambda_1/\Delta t_r U_s, \tag{5}$$

which should then be only a function of the incident Mach number.

An analytic argument is presented in appendix E which shows that not only is the above expression the proper quantity for displaying the data for the reflected shock thickness but also that it is only a function of incident Mach number.

The reciprocal thickness λ_1/δ_r is being used because it is usually the quantity considered in the case of the free running shock (for which case the ratio is more convenient for plotting since $\lambda/\delta \to 0$ for $M_s \to 1$).

Figure 24 presents a plot of the reciprocal thickness for the reflected shock, as defined by equation 5, versus the incident Mach number for the experimental data for argon, nitrogen, and carbon dioxide. The CO_2 data point for $M_s \approx 8$ was plotted to see if the thickness was consistent with the shock thickness at the lower Mach

numbers and not as data to influence heavily a fairing of a thickness versus Mach number curve. The maximum slope thicknesses for the CO_2 data were obtained by using the portion of the reflected shock profile that corresponded to the frozen-frozen pressure jump discussed in the last section, i.e., the present definition of shock profile is restricted to translational and rotational relaxation only and the vibrational part is considered as a separate process. The maximum slope thicknesses for the argon, nitrogen, and carbon dioxide data were based directly on the recorded profiles and no attempt was made to compensate for the effect of heat transfer to the cold end wall.

In plotting the data a consistent definition for the mean free path length had to be chosen. The mean free path length based on viscosity was selected because of the obvious role the transport parameters assume in the problem and because of the desire to compare the data for the reflected shock to the available data for the free running shock (for which case the viscosity is used). The mean free path length in region ① was computed from the relation

$$\lambda = \frac{16}{5}\sqrt{\frac{\gamma}{2\pi}}\ \frac{\mu}{\rho a}$$

for all three gases using the respective room temperature values for the viscosity, density, and speed of sound.

Several observations from figure 24 are of fundamental interest in the present study. The reciprocal shock thickness λ_1 / δ_r is, within a factor of 50 per cent, the same for all three gases and, furthermore, "varies" with incident Mach number in roughly the same way. In addition, there is no striking difference in the thickness between a polyatomic gas like CO_2 and a monatomic gas like argon. This result is quite significant for CO_2 because it indicates that from a gas dynamic point of view there is nothing unusual about the viscous properties of CO_2, i.e., in comparison to argon.

Since a casual inspection of figure 24 may lead one to believe that the measured reflected shock thicknesses are a property of the pressure gauge rather than a valid gas dynamic effect, it should be pointed out that the experimental data involved variations in λ_1 of a factor of four and variations in U_s of a factor of almost three.

A comparison of the reciprocal thickness for the nitrogen data to that for the argon data shows that the value of the reciprocal thickness for nitrogen is roughly 21 per cent greater than that for argon. This is particularly interesting since the measurements reported by Linzer and Horning (Ref. 3) on the reciprocal thickness of the density profile for the free running shock in nitrogen and argon exhibit a reciprocal thickness for nitrogen

approximately 30 per cent greater than that for argon (see Figs. 4 and 5 of Ref. 3).

One could get a rough idea of how important a role heat transfer plays in the reflection of a shock front from a cold wall if one could answer the following question: What is the relationship between the thickness of a reflected shock profile for the case of a heat conducting wall to the thickness of a reflected shock profile for the case of a thermally insulated wall?

In order to settle the above question in detail, one would also need experimental results for the case of the thermally insulated wall. Unfortunately this is not feasible experimentally. Nevertheless, a rough idea can be obtained by comparing the reciprocal thickness of the reflected shock profile to the reciprocal shock thickness of, say, the incident shock pressure profile. If the reflected shock profile is much thicker than the incident shock profile, then one can conclude that heat conduction dominates the reflection process; but if they are roughly of the same order, then heat conduction to the cold end wall must play only a minor role in the process.

Although a large amount of work has been done with the free running shock, it can by no means be considered a closed question as to which theory gives the best prediction for the physical problem (not to reported

experimental results.) Nevertheless, it is generally agreed that if one uses the proper Prandtl number, the proper exponent in the viscosity law $\mu \sim T^{\omega}$, and the profile for the proper flow variable, then the solution to the Navier-Stokes equations gives a thickness that is within, at most, a factor of two of reported experimental results for argon. Since we are interested in general results and since the Navier-Stokes equations give a shock thickness for all Mach numbers, the Navier-Stokes equations will be used as a source of information for the incident shock in argon.

Figure 25 presents the results of some computations carried out by Chahine (Ref. 23) using the Navier-Stokes equations and the method proposed by Gilbarg and Paolucci (see Ref. 24). The properties of argon were approximated by assuming a viscosity law $\mu \sim T^{\omega}$, a gas constant $\gamma = 5/3$, and a Prandtl number $P_r = 2/3$ for the computations. The computations were carried out on an IBM 7090 for five different Mach numbers and three values of the exponent in the viscosity law. (The computed points are designated by the symbol $\times$ in figure 25.) The shock thicknesses plotted in figure 25 are based on the maximum slope of the pressure profile.

For argon the value of ω varies from around 0.82 for low temperatures to around 0.75 for high temperatures.

Therefore, according to figure 25, the reciprocal shock thickness for the incident shock varies from a maximum of about 0.36 at $M_s = 4$ to about 0.30 at $M_s = 10$ and $M_s = 2.5$. Comparing this to the reciprocal thickness for a reflected shock in argon, figure 24, we find that the reflected profile is about 46 per cent thicker at $M_s = 4$, and only about 22 per cent thicker at $M_s = 8$.

For incident shock Mach numbers approaching 1, there is no question that the reflection process should reduce to a simple acoustic reflection and that the reciprocal thickness for the reflected shock should merge with the reciprocal thickness for the incident shock. However for the high Mach number range, where effects of heat transfer should appear, there seems to be no indication that the reflection process (within the shock front) is dominated by the heat transfer to the cold end wall. In fact, the reflected shock thickness for argon is so close to the thickness for the incident shock that one may wonder whether or not shock thickness (in general) is a sufficiently sensitive quantity for study.

Although no conclusions can be drawn at present, it is interesting to compare the data for argon and nitrogen in figure 24 to the data presented in figures 10 and 11 respectively for reference 4. The close similarity between the results for the two apparently different

problems indicates that there is much to be learned concerning the shock reflection process.

APPENDIX A

DISTURBING INFLUENCES ON THE ONE-DIMENSIONAL FLOW NEAR THE PRESSURE GAUGE

The disturbing effect on the desired one-dimensional flow in the reflected region near the pressure gauge due to the boundary layer behind the incident shock and the non-planar shape of the incident shock will be considered in this appendix.

The boundary layer which forms behind the incident shock causes a disturbance in the reflected region due to the fact that the reflected shock must propagate into a non-uniform flow field. The disturbance which is thus created in the reflected region near the wall of the shock tube propagates radially inward with a velocity equal to the speed of sound in region ⑤. Since the Mach number of the reflected shock, based on the sound speed in the reflected region, is always subsonic and is bounded by the limits

$$\sqrt{\frac{2}{2+\alpha}} < M_R \leq 1$$

where

$$\alpha = (\gamma+1)/(\gamma-1) \quad ,$$

then the extent of the region of influence of any disturbance originating at the wall of the shock tube can, at most, be only several times the thickness of the reflected region at any given time. It is evident from figure 2 that such a disturbance can have no influence on the flow near the pressure gauge for the duration of the present experiment (5 μsec).

The more important consideration is the non-planar shape of the incident shock wave. Precise details regarding shock curvature are not entirely clear but some approximate statements can be made with regard to the GALCIT 17-in.-diameter low-pressure shock tube which will suffice here. The amount of curvature in the incident shock surface is greater for lower initial pressures (true for low pressures only). Therefore the largest perturbation to the one-dimensional flow in the reflected region should occur for the runs at the lowest initial pressures. Reference 14 reports the results of some experimental measurements in the GALCIT 17-in.-diameter shock tube on the amount of shock curvature for initial pressures of 30, 50, 70, and 100 μ Hg in argon. The data for the lowest pressure shows that the departure from a plane surface for the incident shock amounts to about 11 mm over the 17 inch diameter of the shock tube. A rough reconstruction of the incident shock shape (from the data of reference 14) is

shown in figure 2 for an initial pressure of 30 μHg.

Since the pressure gauge samples a core of gas 1 3/8" in diameter (see figure 2), a rough measure for estimating the effect on the reflected shock profile data can be obtained by comparing the ratio of the shock curvature at the outer edge of the gauge ($\approx$0.02 mm) to the gauge sampling length in the incident flow ($\approx$10 mm if taken conservatively as the incident shock thickness at an initial pressure of 30 μHg). This gives a ratio somewhat less than 0.5 per cent. Therefore one would not expect the reflected shock profile data (for initial pressures around 30 μHg) to be off by more than, say, one per cent due to shock curvature in the GALCIT 17-in.-diameter shock tube.

For higher initial pressures ($\approx$1 mm Hg) there is reason to believe that the shape of the shock surface does not continue to become more and more planar with increasing initial pressure but that a lower limit to the deviation of about one millimeter exists for the GALCIT 17-in.diameter shock tube.* Therefore the profile data would be in error by several per cent due to shock curvature for initial pressures above 1 mm Hg (below 1 mm Hg shock curvature can be assumed, like shock thickness, to scale inversely with

*Conclusion drawn from some recent experiments on shock curvature conducted by R. M. Bowman in the GALCIT 17-in.-diameter shock tube.

pressure). However, this is not the limiting element in the present study because shock profile data for initial pressures above 500 μHg can not be obtained due to the lower limit on the resolution time of the pressure gauge (see Ref. 1).

The error introduced into the heat transfer data or the relaxation data for CO_2 (which were obtained at higher initial pressures than for reflected shock profile data) due to the one millimeter of shock surface deviation would be a fixed value and of the order of the risetime of the pressure gauge.

APPENDIX B

DETAILS OF THE PRESSURE GAUGE CIRCUIT AND EQUIPMENT

A schematic drawing of the details of the pressure gauge circuit is presented in figure 26. Since the pressure gauge contains a capacitive type sensing element, it is represented by a variable capacitor in the figure. The important elements of the circuit should be noted at this point. The grid resistor of the first stage of the RHS amplifier (RHS Electronics model 201, designed by R. H. Swartley) was replaced by a 1.8 MΩ resistor in order to minimize the RC decay of the output signal from the gauge circuit. The coaxial cables denoted by A and B in the figure were made less than 6 inches in length in order to minimize the capacitive loading on the pressure gauge. This was necessary because any capacitance in parallel with the gauge capacitor ($C_1 \approx 100$ μμf) would reduce the output from the gauge and it was desired that the sensitivity of the gauge be held to as large a value as possible. The short cable lengths were achieved by mounting both the amplifier and the gauge circuit box ② near the end wall of the shock tube. (In cases where an amplifier in the shock tube console was used, the added coaxial cable length (≈ 9') reduced the sensitivity of the gauge by a

factor of two.)

During a run a steady DC voltage for the gauge was obtained from a 1/2 μf (7.5 kV) capacitor C_3 which was charged to the desired level by a variable voltage power supply. A variable output voltage was obtained from a 15 kV power supply (Del Electronics Corp., model 15-1-6) by varying the input voltage to the power supply. The gauge voltage was monitored during a run with an electrometer voltmeter (Keithley Instruments, model 600A) through a 1000:1 ratio divider probe (Keithley Instruments, model 6103A).

It was found necessary to add the resistor R_3 to the circuit to filter an unacceptably large 60 cycle signal which was being picked up by an unshielded terminal at which the gauge voltage was being monitored. The gauge circuit was discharged through the switch S_2 after each run for both purposes of safety and as protection to the pressure gauge.

Since the sensitivity of the gauge is proportional to the applied voltage (Ref. 1), a maximum voltage is desirable for measurements of weak pressure signals. The maximum voltage applied to the particular gauge used to collect the present data (Lexan polycarbonate plastic rod with 0.003" electrode separation) was 3.6 kV. Type RG-62/U coaxial cable was found quite adequate for

handling the 3.6 kV between the various units. (Some tests with a different gauge were run at 5 kV.) However, special care was needed in constructing the cable connections to eliminate arcing. Figure 27 shows some details of the pressure gauge housing and an example of a typical connection used to eliminate arcing.

Experience has shown that for a minimum acceptable signal to noise ratio the weakest signal that can be displayed on an oscilloscope is about 0.5 mv/div (before amplification). Using a gauge voltage of 3 kV, the above gauge sensitivity gives a value of 10 mm Hg/div as a lower practical limit for displaying a pressure signal.

Some patience has been needed with the present design of the pressure gauge because, for the more sensitive settings of the oscilloscope, the "zero output" from the gauge would fluctuate appreciably during a run. At first, this was attributed entirely to sporadic breakdown of the dielectric material in the gauge capacitor due to the large impressed voltage gradient ($\approx$1 kV/mil). However, later runs using higher driver pressures ($\approx$80 psia versus 20 psia) amplified the effect, indicating that the stress waves which are produced by the diaphragm opening process and which travel down the shock tube wall ahead of the shock enter the housing of the pressure gauge and set up a pattern of stress waves in the Lexan rod which show up as

fluctuations of the "zero position'. This problem certainly could have been alleviated had more attention been paid in the gauge design to mechanically isolating the gauge housing from the shock tube end wall.

APPENDIX C

SUMMARY OF JUMP RELATIONS FOR CO_2

The following jump relations for the incident and reflected shocks were used in conjunction with an enthalpy versus temperature diagram for CO_2 (Fig. 14) to compute the quantities displayed in figures 15 through 17. The jump relations were obtained from page 388 of reference 6 (re-derived to account for an arbitrary caloric equation of state in region ①).

Incident Shock:

$$n = \rho_2/\rho_1$$

$$u_2/U_s = (1 - 1/n)$$

$$p_2/p_1 = 1 + \frac{U_s^2}{p_1/\rho_1}(1 - 1/n)$$

$$h_2/h_1 = 1 + \frac{U_s^2}{2h_1}(1 - 1/n^2)$$

Reflected Shock:

$$5 = \rho_5/\rho_1$$

$$U_R/U_s = (n-1)/(5-n)$$

$$p_5/p_1 = 1 + \frac{U_s^2}{p_1/\rho_1}\frac{(n-1)(5-1)}{5-n}$$

$$h_5/h_1 = 1 + \frac{U_s^2}{h_1}\frac{(n-1)(5-1)}{(5-n)\,n}$$

Since one can use the perfect gas relation $P = \rho RT$ for CO_2 in region ① , then

$$p_1/\rho_1 = RT_1 = \frac{1}{\gamma}(\gamma RT_1) = \frac{1}{\gamma} a_1^2 ,$$

and

$$\frac{U_s^2}{p_1/\rho_1} = \gamma \frac{U_s^2}{a_1^2} = \gamma M_s^2 .$$

Therefore one can use γM_s^2 for the coefficient in the pressure jump relation as long as the values used for γ and M_s are consistent.

Expressing the enthalpy as a sum of two parts, we have for CO_2 at room temperature

$$h_1 = \frac{7}{2} RT_1 + h_{vib}$$

or

$$h_1 = \left[\frac{7}{2} + (h/RT_1)_{vib}\right] RT_1$$

$$= \left[\frac{7}{2} + 0.26\right] RT_1$$

$$= 3.76\ RT_1 .$$

Therefore

$$h_1 = \frac{3.76}{\gamma}(\gamma R T_1) = \frac{3.76}{\gamma} a_1^2 ,$$

and

$$\frac{U_s^2}{h_1} = \frac{\gamma}{3.76} M_s^2 ,$$

where again the values used for γ and M_s must be consistent.

APPENDIX D

RATIO OF RELAXATION TIMES τ_2/τ'_2

An approximate analysis for computing the ratio of relaxation times τ_2/τ'_2 for a reflected shock in CO_2 will be discussed in this appendix.

Figure 28 presents a scale drawing of an x-t diagram for a reflected shock in CO_2, for the case $M_s = 5$ (based on $\gamma = 7/5$), and defines the relevant quantities in the flow field for the following analysis.

When a particle of gas in region ① is first intercepted by the incident shock, it moves with the frozen speed, i.e., value of u_2 for $\gamma = 7/5$. Later in time, when the particle reaches vibrational equilibrium, it moves with the equilibrium speed which in laboratory coordinates is faster. Therefore, the actual trajectory of the particle of gas must lie between the corresponding trajectories for the two velocities. This is shown in figure 28. For very short times the particle trajectory can be approximated with the frozen speed, and for very long times it can be approximated with the equilibrium speed. However, for a time equal to the relaxation time in region ②, a reasonable approximation is the average between the two speeds.

The state of the gas at the terminal end of the trajectory in region ② is such that its temperature is lower, its density is greater, and it is moving more rapidly. Each of these factors contribute to the strengthening of the reflected shock at that point. Therefore a positive pressure wave is produced at the shock and propagates back towards the end wall with the local speed of sound in region ⑤; the resulting pressure history on the end wall then gives an approximate measure for the relaxation time τ_2 (see Fig. 28). Since most of the trajectory for the pressure pulse traveling through the gas in region ⑤ is nearly in the state determined by the jump E② - E⑤, an acceptable approximation to the trajectory is a constant speed of sound a^*_5 equal to the speed of sound in region ⑤ for equilibrium conditions. The data of figures 15 through 17 was used to compute a^*_5 and the velocity behind the incident shock u_2. These quantities are presented in figure 29 as a function of incident Mach number. The sound speed a^*_5 was computed from the relation (and consequently defined by):

$$a_5^{*2} = \left(\frac{dp}{d\rho}\right)_{S=const,\ E②-E⑤}$$

$$= \frac{h'}{h'-1} RT_5 ,$$

where

$$h' = \frac{d(h/RT_1)}{d(T/T_1)} .$$

The time the particle of gas spends in region ②, which is designated by τ_2 in figure 28, is determined by the intersection of the particle trajectory and the reflected shock trajectory. The reflected shock speed U_R, for the three different jump conditions, is plotted in figure 30 as a function of incident Mach number. The three values for $M_s = 5$ were used in constructing the x-t diagram of figure 28. Again, the actual trajectory must lie between the frozen and equilibrium speeds. Since it was concluded that the relaxation time in region ⑤ is roughly equal to the time τ'_2 (see section 3.2.3), then for a time roughly equal to τ'_2 the position of the reflected shock can be approximated by the average between the frozen and equilibrium speeds.

If we define the following dimensionless average velocities

$$\bar{u}_2 = (u_2/U_s)_{average}$$

$$\bar{u}_R = (U_R/U_s)_{average}$$

$$\bar{a} = a_5^*/U_s ,$$

then the following results can be obtained from a simple geometrical analysis

$$\tau_2' = (1 + \bar{u}_r)/(\bar{u}_2 + \bar{u}_r)$$

$$\tau_2 = (\tau_2' - 1)(\bar{a} + \bar{u}_r)/\bar{a} \ .$$

The above equations were used to compute the ratio τ_2/τ_2' which is presented as a function of incident Mach number in figure 18.

APPENDIX E

SCALING LAW FOR THE REFLECTED SHOCK PROFILE

The one-dimensional nonsteady motion of a thermally and calorically perfect gas is defined by the following set of equations:

$$\frac{\partial \rho}{\partial t} + \frac{\partial \rho u}{\partial x} = 0$$

$$\frac{\partial \rho u}{\partial t} + \frac{\partial}{\partial x}\left[p + \rho u^2 - \tau\right] = 0$$

$$\frac{\partial}{\partial t}\left[\rho\left(h + \tfrac{1}{2}u^2\right) - p\right] + \frac{\partial}{\partial x}\left[\rho u\left(h + \tfrac{1}{2}u^2\right) - u\tau + q\right] = 0$$

$$p = \rho R T$$

$$h = c_p T \quad ,$$

If, in addition, the Navier-Stokes approximations are used

$$\tau = \bar{\mu}\,\frac{\partial u}{\partial x}$$

$$q = -k\,\frac{\partial T}{\partial x} \quad ,$$

where $\bar{u}$ and k are assumed to be known functions of tempera-

ture, then the set is complete and in principle could be solved given proper boundary conditions.

For the shock reflection problem, the problem is properly posed if one defines the thermal behavior of the wall (heat conducting or thermally insulated), the initial conditions in region ①, the incident shock Mach number M_s, and the position of the incident shock profile (profile assumed known from the steady solution).

The flow variables can be non-dimensionalized by the quantities in region ① as follows

$$\tilde{\rho} = \rho/\rho_1 \qquad \tilde{h} = h/h_1$$

$$\tilde{u} = u/a_1 \qquad \tilde{T} = T/T_1$$

$$\tilde{p} = p/p_1 ,$$

and the above set of equations then become

$$\frac{\partial \tilde{\rho}}{\partial t} + a_1 \frac{\partial \tilde{\rho}\tilde{u}}{\partial x} = 0$$

$$\frac{\partial \tilde{\rho}\tilde{u}}{\partial t} + a_1 \frac{\partial}{\partial x}\left[\frac{1}{\gamma}\tilde{p} + \tilde{\rho}\tilde{u}^2 - \frac{\gamma}{\rho_1 a_1^2}\right] = 0$$

$$\frac{\partial}{\partial t}\left[\tilde{\rho}\left(\frac{\tilde{h}}{\gamma-1} + \frac{1}{2}\tilde{u}^2\right) - \frac{1}{\gamma}\tilde{p}\right] + a_1 \frac{\partial}{\partial x}\left[\tilde{\rho}\tilde{u}\left(\frac{\tilde{h}}{\gamma-1} + \frac{1}{2}\tilde{u}^2\right) - \frac{\gamma}{\rho_1 a_1^2}\tilde{u} + \frac{\gamma}{\rho_1 a_1^3}\right] = 0$$

$$\tilde{p} = \tilde{\rho}\tilde{T}$$

$$\tilde{h} = \tilde{T}$$

$$\tau = a_1 \bar{\mu} \frac{\partial \tilde{u}}{\partial x}$$

$$q = -\frac{a_1^2}{\gamma - 1} \frac{k}{c_p} \frac{\partial \tilde{h}}{\partial x} .$$

The x and t derivatives operating on the first three equations can be made non-dimensional by any length and time scale ($\tilde{x} = x/X$ and $\tilde{t} = t/T$) provided

$$X / T = a_1 .$$

However, only one definition of X will non-dimensionalize the viscous term in the momentum equation and the energy equation, i.e.,

$$X = \bar{\mu}_1 / \rho_1 a_1 .$$

If we introduce the Prandtl number

$$P_r = \bar{\mu} c_p / k ,$$

and define

$$\tilde{\mu} = \bar{\mu} / \bar{\mu}_1 ,$$

then the expression for the heat conduction term in the energy equation (which is also non-dimensionalized by X) simplifies and the set becomes

$$\frac{\partial \tilde{\rho}}{\partial \tilde{t}} + \frac{\partial \tilde{\rho}\tilde{u}}{\partial \tilde{x}} = 0$$

$$\frac{\partial \tilde{\rho}\tilde{u}}{\partial \tilde{x}} + \frac{\partial}{\partial \tilde{x}}\left[\frac{1}{\gamma}\tilde{p} + \tilde{\rho}\tilde{u}^2 - \tilde{\mu}\frac{\partial \tilde{u}}{\partial \tilde{x}}\right] = 0$$

$$\frac{\partial}{\partial \tilde{t}}\left[\tilde{\rho}\left(\frac{\tilde{h}}{\gamma-1} + \frac{1}{2}\tilde{u}^2\right) - \frac{1}{\gamma}\tilde{p}\right] + \frac{\partial}{\partial \tilde{x}}\left[\tilde{\rho}\tilde{u}\left(\frac{\tilde{h}}{\gamma-1} + \frac{1}{2}\tilde{u}^2\right) - \tilde{\mu}\left(\tilde{u}\frac{\partial \tilde{u}}{\partial \tilde{x}} + \frac{1}{(\gamma-1)P_r}\frac{\partial \tilde{T}}{\partial \tilde{x}}\right)\right] = 0$$

$$\tilde{p} = \tilde{\rho}\tilde{T}$$

$$\tilde{h} = \tilde{T}$$

Therefore, if $\tilde{\mu}$ and P_r are known functions of the dimensionless temperature $\tilde{T}$, the above set of equations will, in principle, give a specific solution for the flow field for a given incident Mach number, i.e.,

$$\tilde{P}_{xx} = -\tilde{p} + \tilde{\tau} = \tilde{P}_{xx}(\tilde{x}, \tilde{t}, M_s).$$

On the wall the time history of the x component of the dimensionless stress tensor becomes (cf. equation 1):

$$\tilde{P}_{xx} = \tilde{P}_{xx}(\tilde{t}, M_s).$$

Defining the maximum slope thickness in the usual way from the dimensionless stress tensor, we have

$$\Delta\tilde{t} = \Delta\tilde{P}_{xx} \Big/ \left(\frac{d\tilde{P}_{xx}}{d\tilde{t}}\right)_{max} = g(M_s).$$

Therefore the dimensionless thickness is a function of

incident Mach number only. In terms of physical time the thickness becomes:

$$\Delta t = T g(M_s) = \frac{X}{a_1} g(M_s) = \frac{X}{U_s} M_s g(M_s).$$

From the relation

$$\mu = \frac{1}{2} \rho \bar{c} \lambda ,$$

we get

$$X = \frac{\bar{\mu}_1}{\rho_1 a_1} = \frac{1}{2} \left(\frac{\bar{\mu}_1}{\mu_1}\right)\left(\frac{\bar{c}_1}{a_1}\right) \lambda_1 = C \lambda_1 .$$

Absorbing the constant into a new function of M_s, we have

$$\Delta t = \frac{\lambda_1}{U_s} G(M_s) ,$$

or

$$\lambda_1 / \Delta t U_s = 1 / G(M_s) ,$$

which is the dimensionless quantity considered in equation 5.

REFERENCES

1. Baganoff, D. "Pressure gauge with one-tenth microsecond risetime for shock reflection studies." Rev. Sci. Instr., Vol. 35 (1964) pp. 288-295.

2. Sherman, F.S. "A low-density wind-tunnel study of shockwave structure and relaxation phenomena." NACA TN 3298 (1955).

3. Linzer, M., and Horning,D.F. "Structure of shock fronts in argon and nitrogen." Physics of Fluids, Vol. 6 (1963) pp. 1661-1668.

4. Camac, M. "Argon and nitrogen shock thicknesses." Avco-Everett Res. Lab., R. R. 172, December 1963.

5. Wray, K.L.,and Freeman, T.S. "Shock front structure in O_2 at high Mach numbers." Avco-Everett Res. Lab., R. R. 169, November 1963.

6. Liepmann, H. W. and Roshko, A. Elements of Gasdynamics, John Wiley and Sons, Inc., New York (1957).

7. Goldsworthy, F.A. "The structure of a contact region, with application to the reflexion of a shock from a heat-conducting wall." Jour. Fluid Mech., Vol. 5 (1959) pp. 164-176.

8. Slachmuylders, E. "Measurements of the acceleration of reflected shock waves by means of a new heat transfer gauge." Aeronautical Engineering thesis, Calif. Inst. of Tech. (1963).

9. Sturtevant, B. "End-wall heat-transfer effects on the trajectory of a reflected shock wave." To be published (Physics of Fluids).

10. Clarke, J.F. "Heat conduction through a polyatomic gas." The College of Aeronautics Cranfield, Rept. no. 149, May 1961.

11. Spence, D.A. "Unsteady shock propagation in a relaxing gas." Proc. Roy. Soc. (London) Vol. 264 (1961) pp. 221-234.

REFERENCES (contd.)

12. Bashenova, T.V., and Saytzev, S.G. "Effects of dissociation on the parameters of reflected shock waves in carbon dioxide." Eighth Symposium on Combustion, The Williams and Wilkins Co., Baltimore (1962) pp. 340-344.

13. Liepmann, H.W., Roshko, A., Coles, D., and Sturtevant, B. "A 17-inch diameter shock tube for studies in rarefied gasdynamics." Rev. Sci. Instr., Vol. 33 (1962) pp. 625-631.

14. Johnson, D.S. "I. Design and application of piezoceramic transducers to transient pressure measurements. II. Some measurements of curvature and thickness of reflecting normal shocks at low initial pressures." Aeronautical Engineering thesis, Calif. Inst. of Tech. (1962).

15. Clarke, J.F. "On the sudden contact between a hot gas and a cold solid." The College of Aeronautics Cranfield, Rept. no. 124, January 1960.

16. Kubota, T. Private communication (1963).

17. Amdur, I., and Mason, E.A. "Properties of gases at very high temperatures." Physics of Fluids, Vol. 1 (1958) pp. 370-383.

18. Bethe, H.A., and Teller, E. "Deviations from thermal equilibrium in shock waves." BRL Rept. X-117, Aberdeen Proving Ground, Md., (1945).

19. Raymond, J.L. "Thermodynamic properties of the atmosphere of Venus." The RAND Corporation, RM-2292, November 1958.

20. Zienkiewicz, H.K., Johannesen, N.H., and Gerrard, J.H. "Further results on the over-all density ratios of shock waves in carbon dioxide." Jour. Fluid. Mech., Vol. 17 (1963) pp. 267-270.

21. Ferri, A.(Editor) Fundamental Data Obtained From Shock-Tube Experiments, Pergamon Press, New York (1961).

REFERENCES (contd.)

22. Blackman, V. "Vibrational relaxation in oxygen and nitrogen." Jour. Fluid. Mech., Vol. 1 (1956) pp. 61-85.

23. Chahine, M.T. Private communication (1964).

24. Gilbarg, D., and Paolucci, D. "The structure of shock waves in the continuum theory of fluids." Jour. of Rational Mech. and Analysis, Vol. 2 (1953) pp. 617-642.

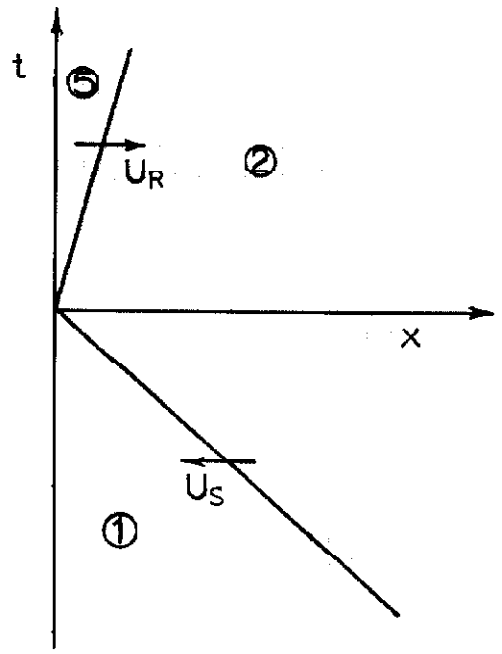

(a) Ideal x-t

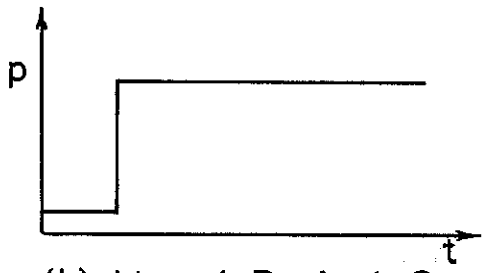

(b) $t/\tau_c \gg 1$, Perfect Gas

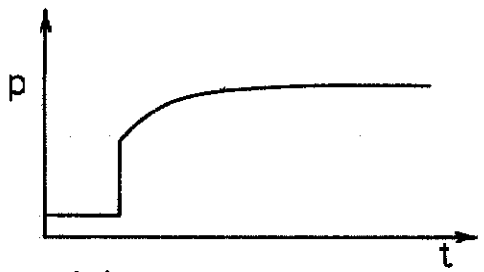

(c) $t/\tau_c \gg 1$, Real Gas

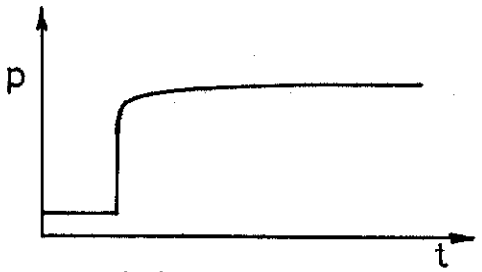

(d) $t/\tau_c \approx 10$

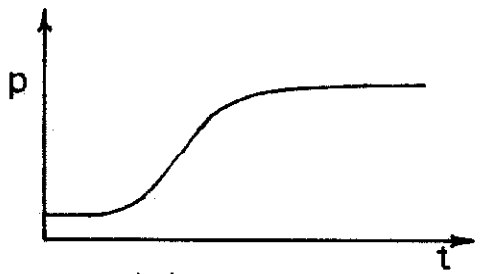

(e) $t/\tau_c \approx 1$

FIGURE 1 x-t DIAGRAM AND END WALL PRESSURE HISTORIES FOR VARIOUS CASES

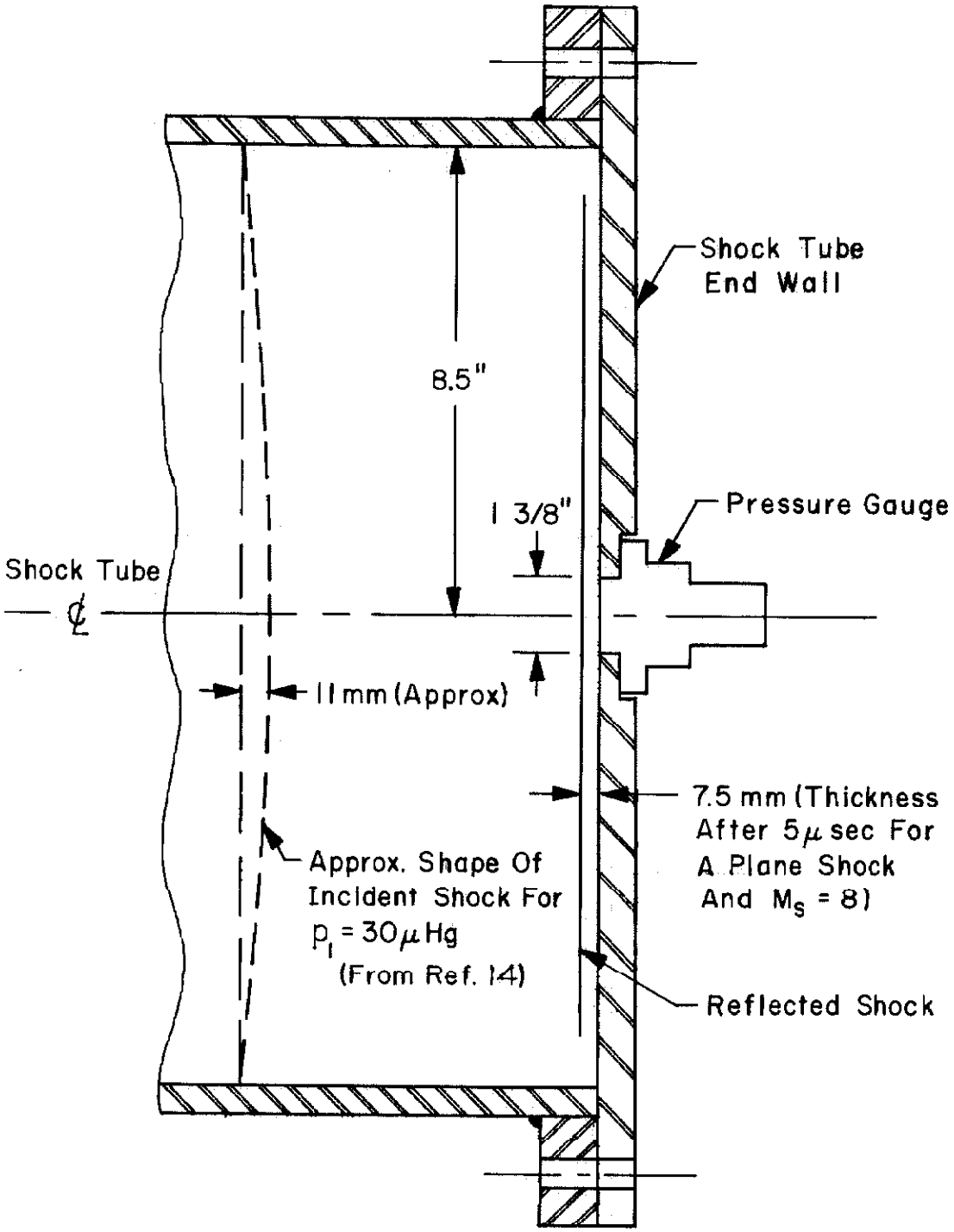

FIGURE 2 RELATIVE DIMENSIONS OF ELEMENTS THAT AFFECT THE EXPERIMENT

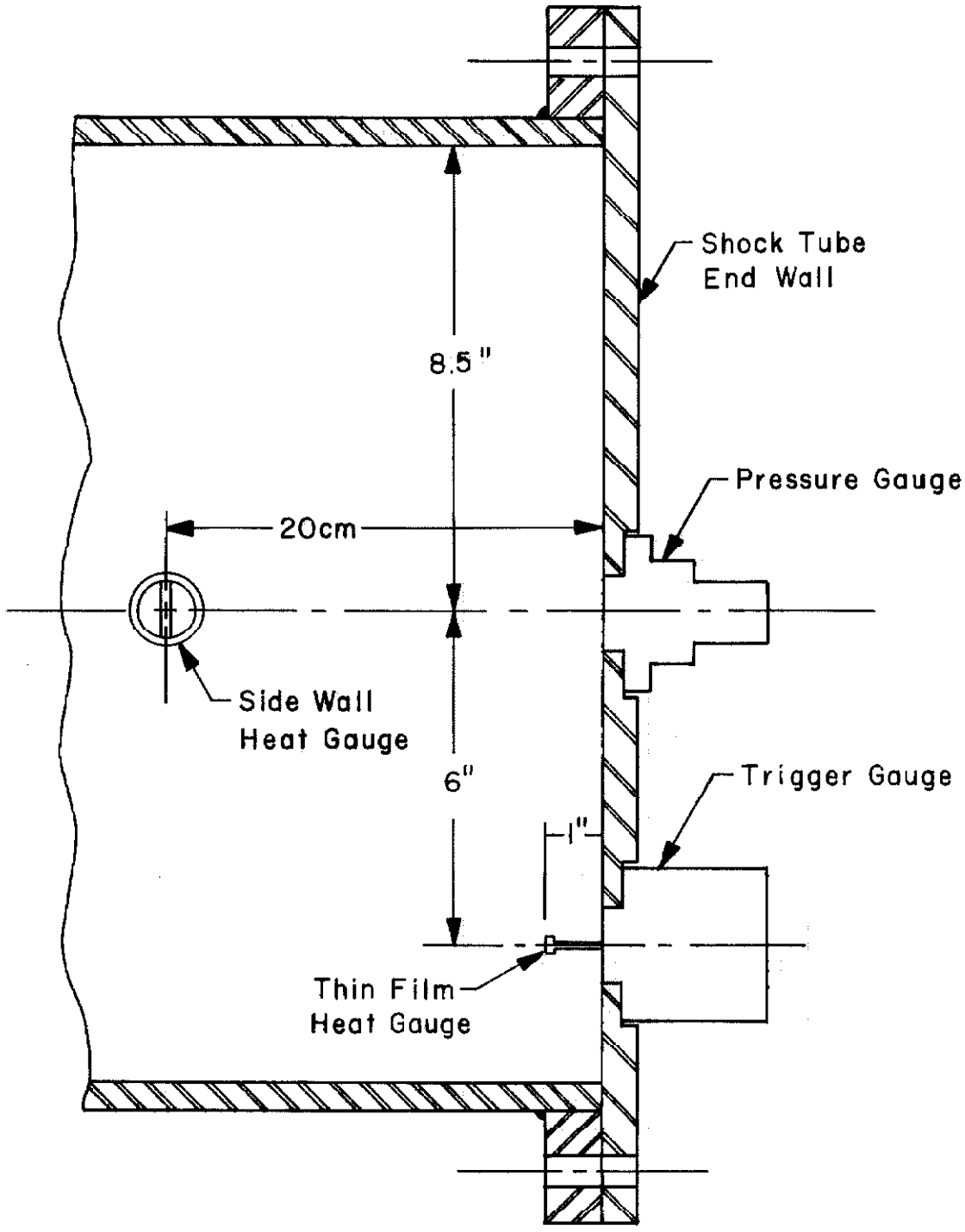

FIGURE 3 LOCATION OF SHOCK TUBE INSTRUMENTATION

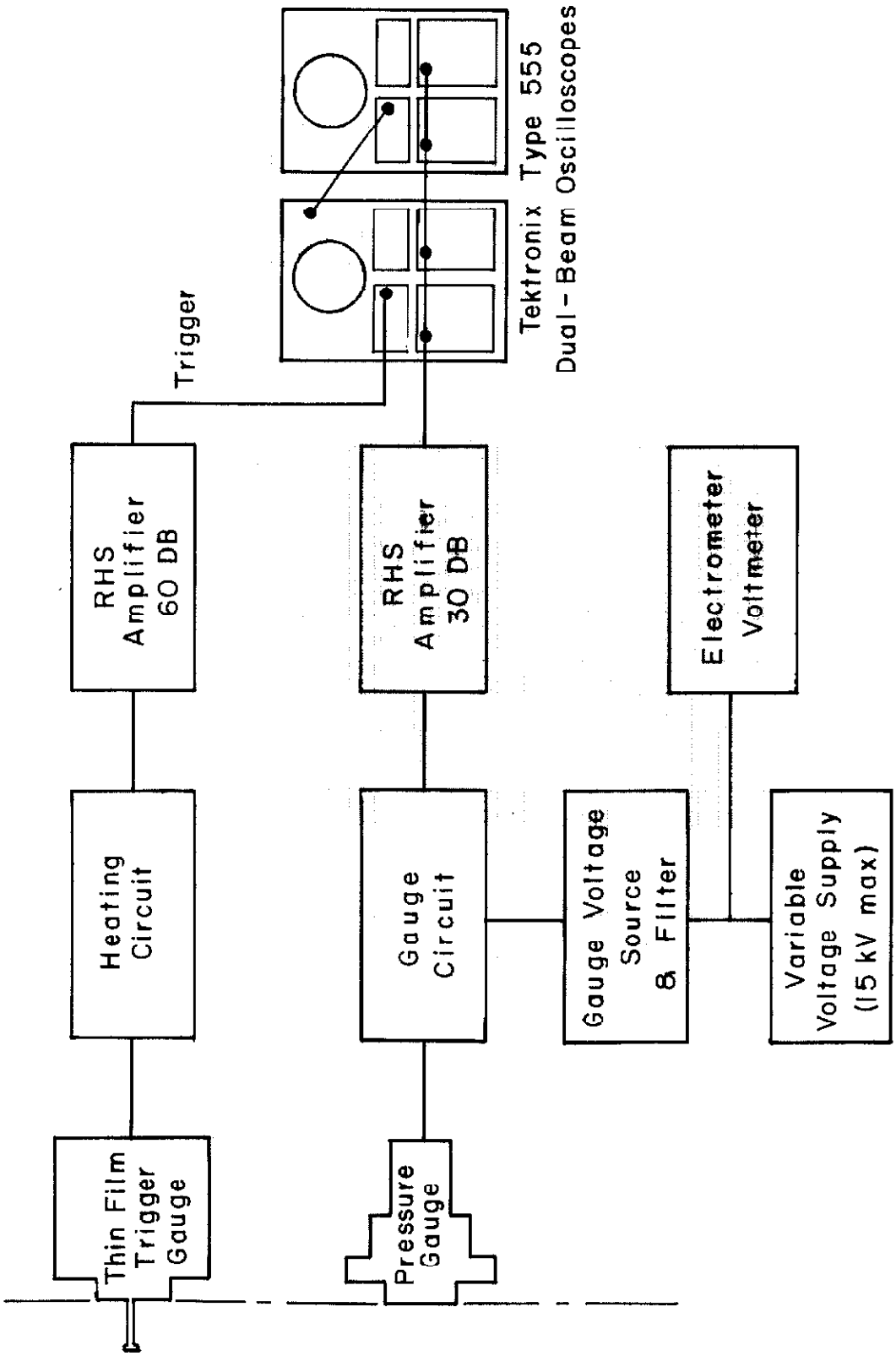

FIGURE 4 BLOCK DIAGRAM OF PRESSURE GAUGE CIRCUIT AND TRIGGER CIRCUIT

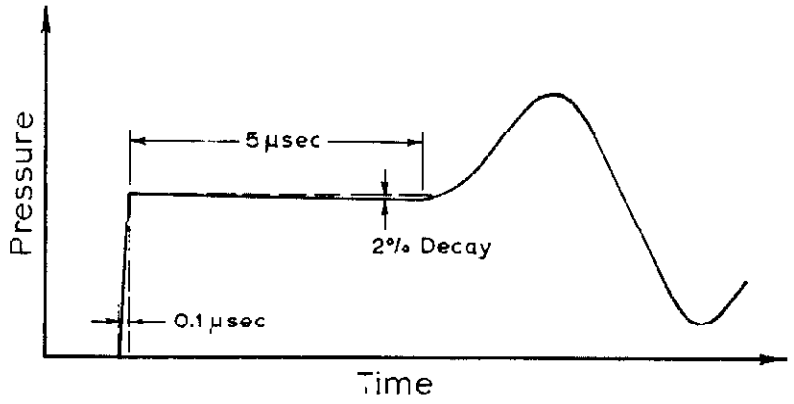

(a) Diagrammatic Description

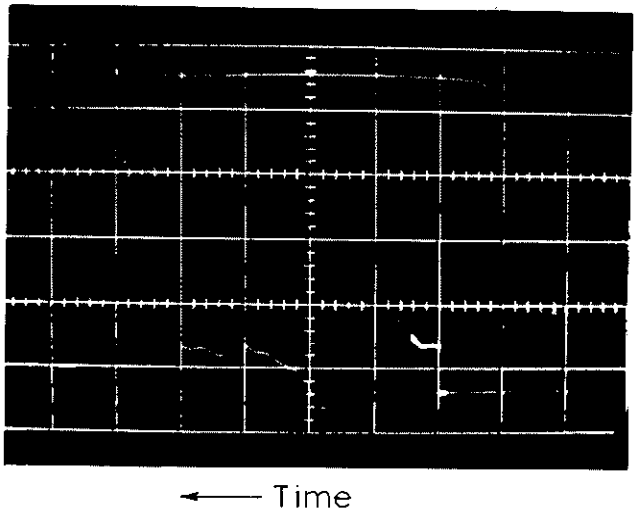

(b) Oscillogram Trace. Driven Gas, Air; $p_1 = 760$ mmHg; $M_s = 1.19$; Upper, 1 μsec/div; Lower, 20 μsec/div.

FIGURE 5 RESPONSE OF PRESSURE GAUGE TO A PRESSURE STEP

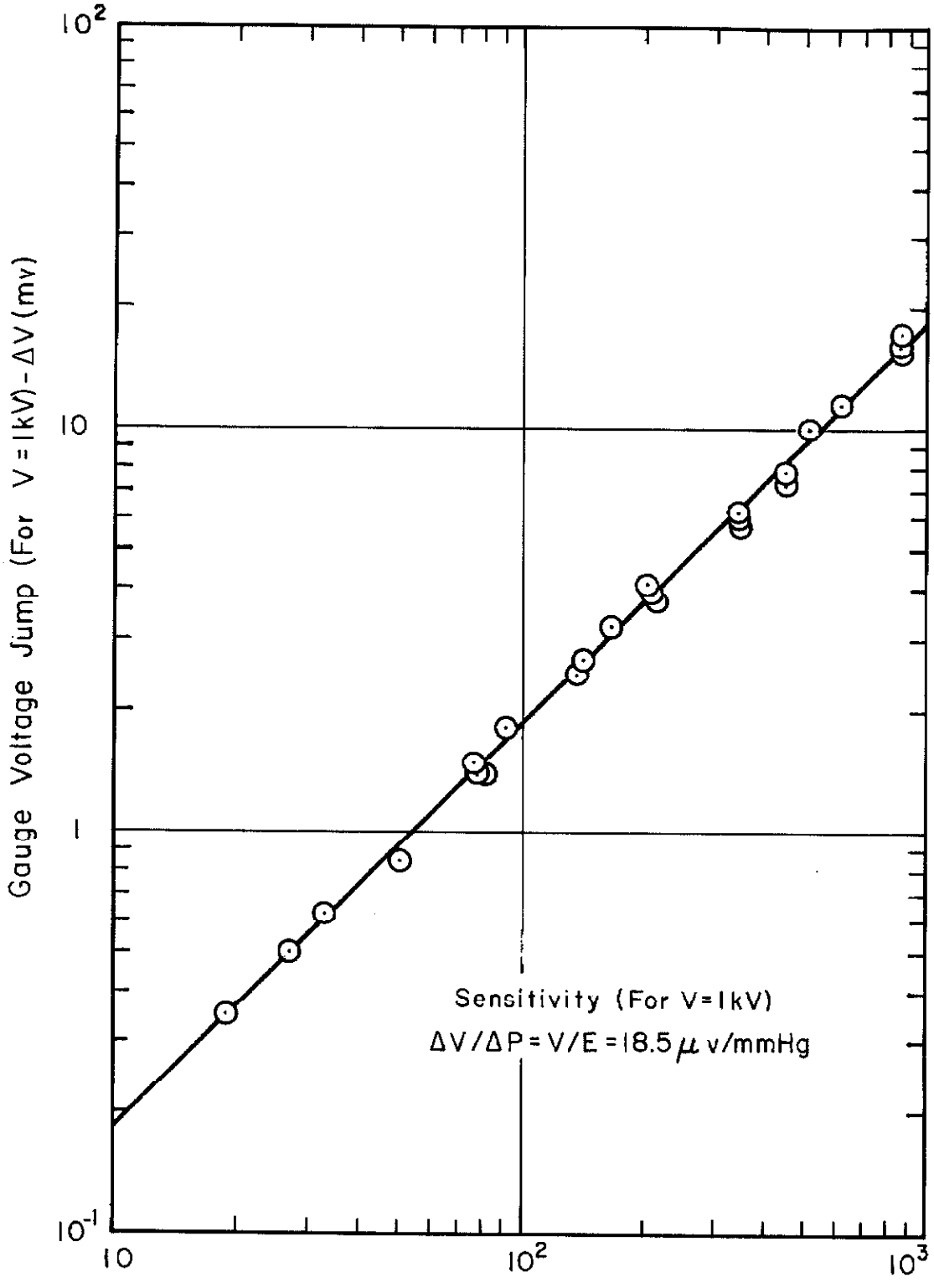

FIGURE 6 PRESSURE GAUGE CALIBRATION

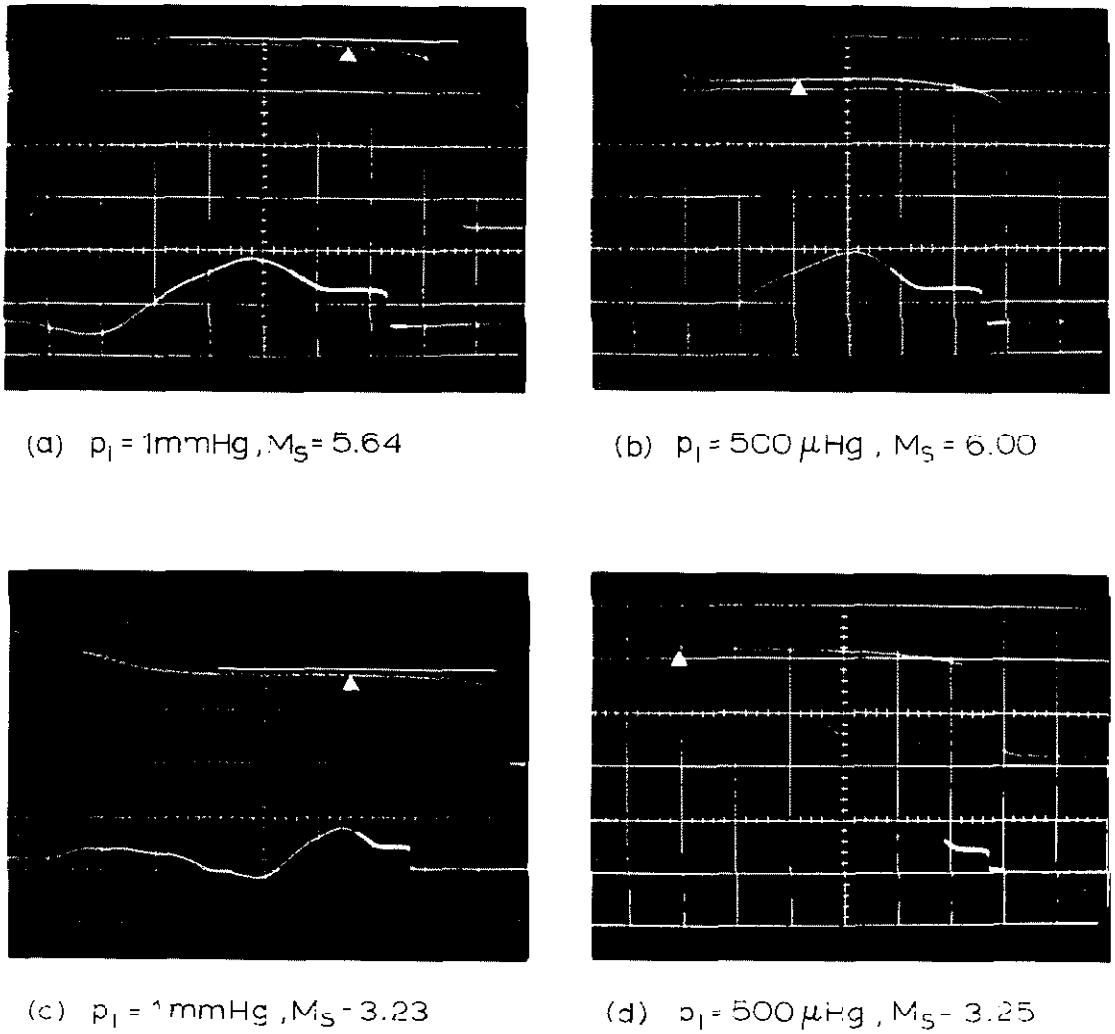

(a) $p_1 = 1 mmHg$, $M_S = 5.64$

(b) $p_1 = 500 \mu Hg$, $M_S = 6.00$

(c) $p_1 = 1 mmHg$, $M_S = 3.23$

(d) $p_1 = 500 \mu Hg$, $M_S = 3.25$

FIGURE 7 EFFECT OF THE THERMAL BOUNDARY LAYER ON THE PRESSURE HISTORIES FOR REFLECTED SHOCKS IN ARGON

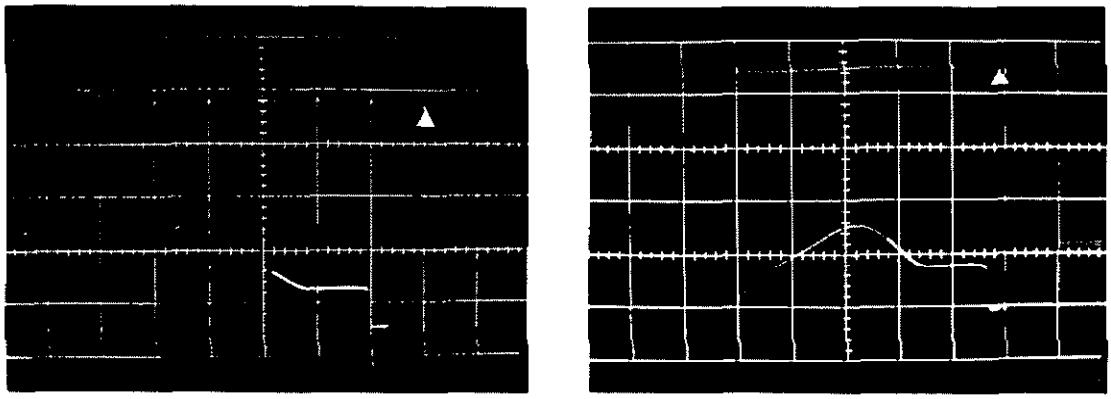

(a) p_1 = 1mmHg , M_S = 5.19

(b) p_1 = 500 μHg , M_S = 5.65

(c) p_1 = 1mmHg , M_S = 3.25

(d) p_1 = 500 μHg , M_S = 3.48

FIGURE 8 EFFECT OF THE THERMAL BOUNDARY LAYER ON THE PRESSURE HISTORIES FOR REFLECTED SHOCKS IN NITROGEN

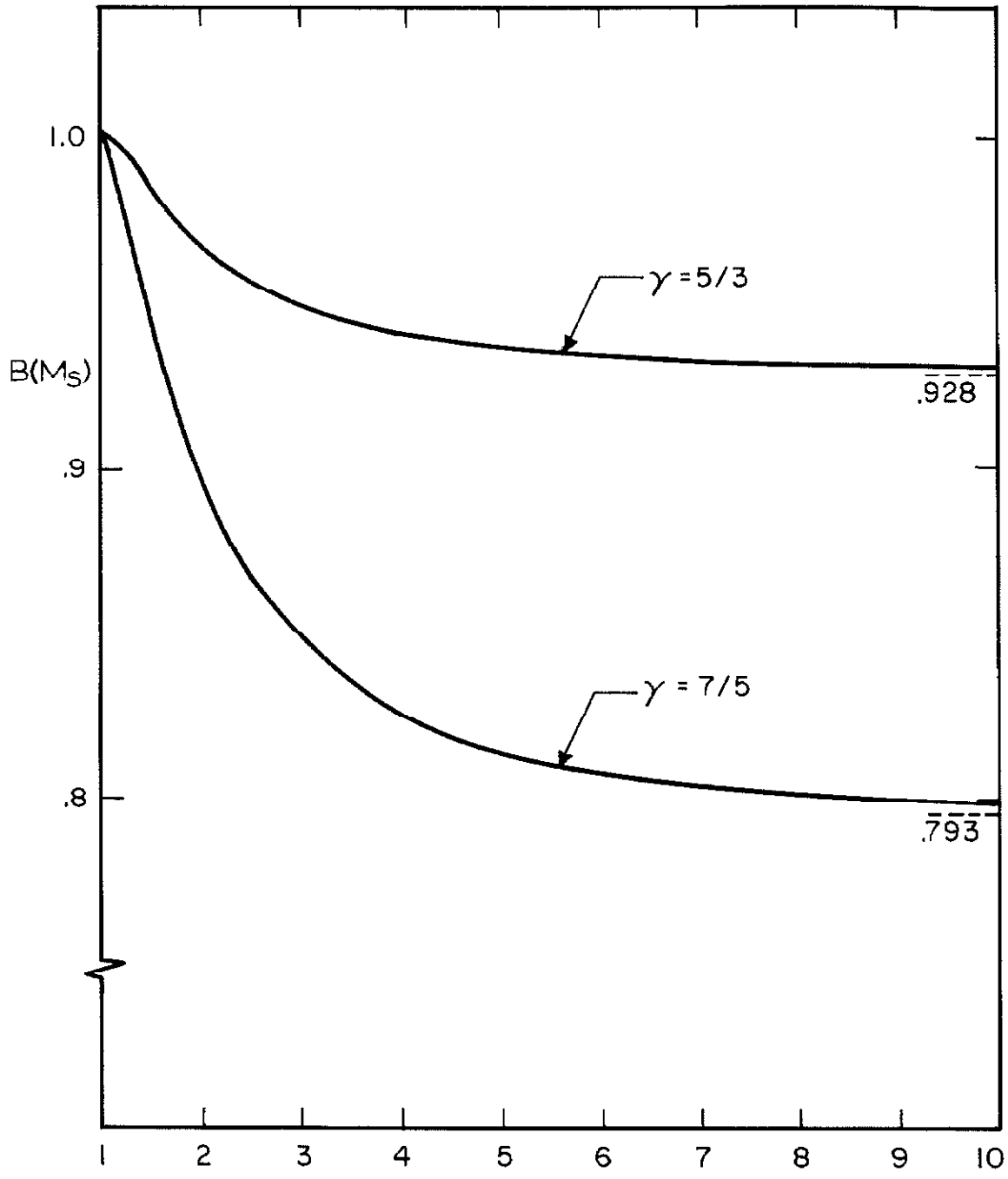

FIGURE 9 COEFFICIENT IN GOLDSWORTHY'S EXPRESSION FOR THE PRESSURE PERTURBATION (EQ.1)

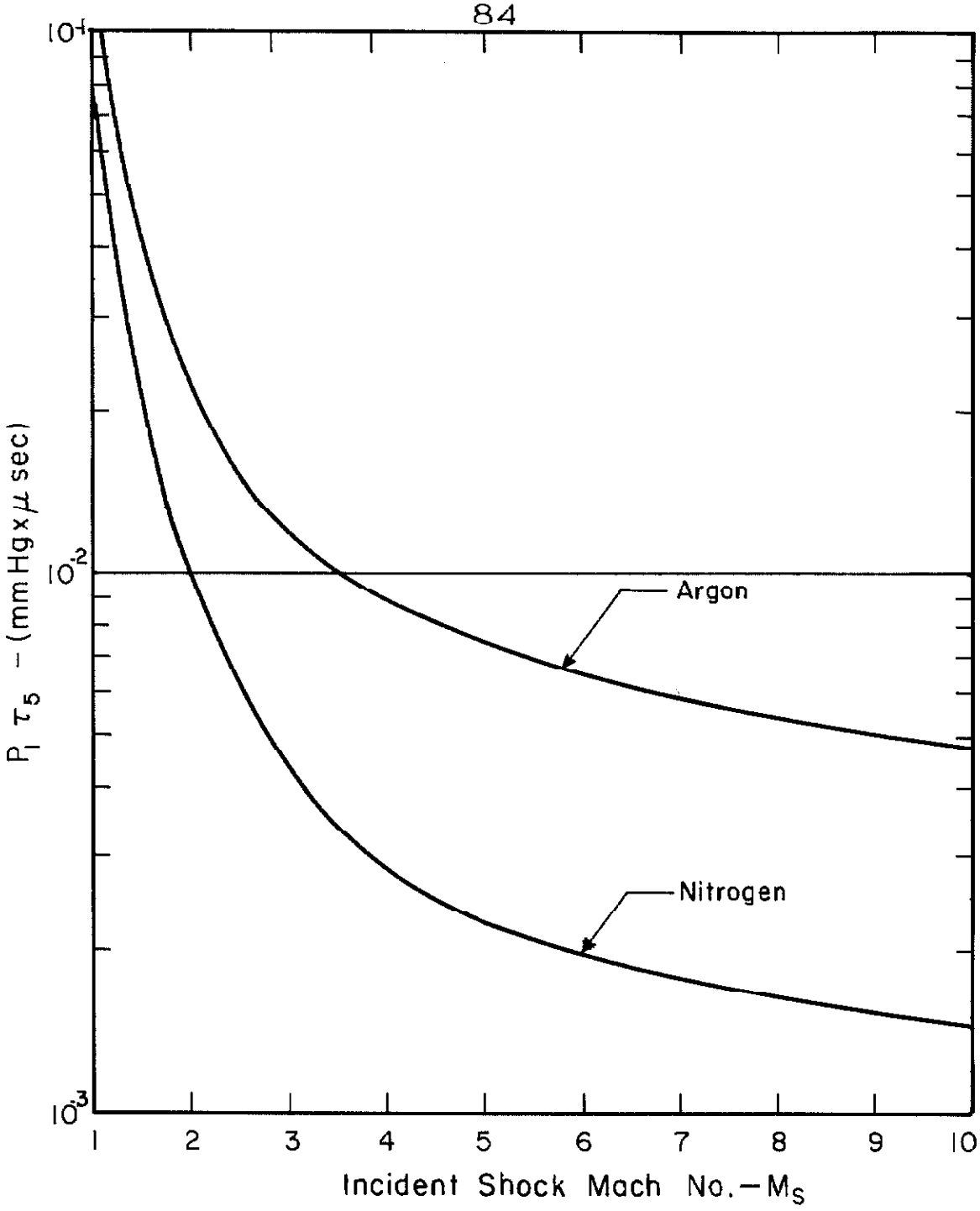

FIGURE 10 CHARACTERISTIC TIME τ_5 FOR ARGON AND NITROGEN

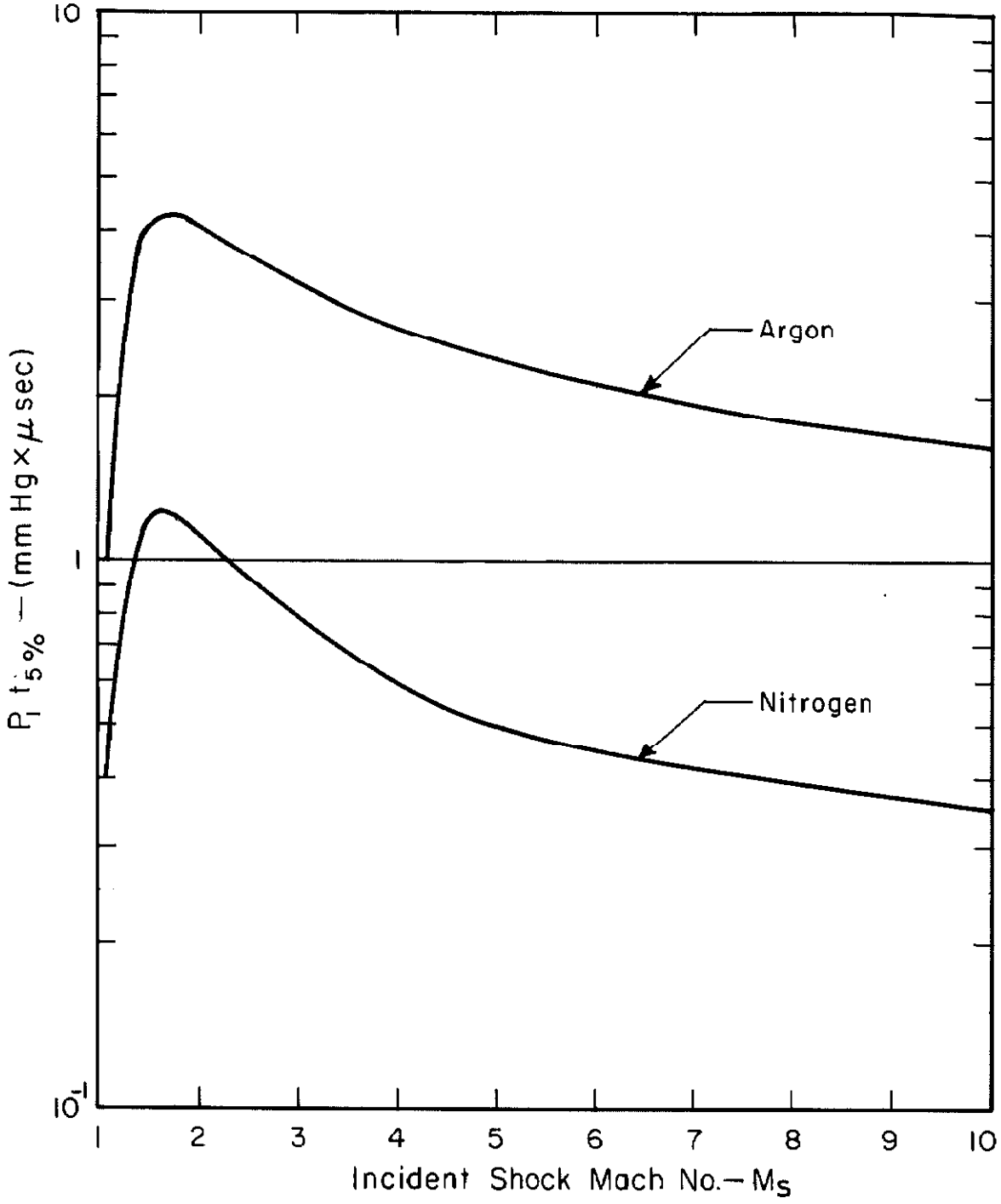

FIGURE 11 $t_{5\%}$ FOR ARGON AND NITROGEN

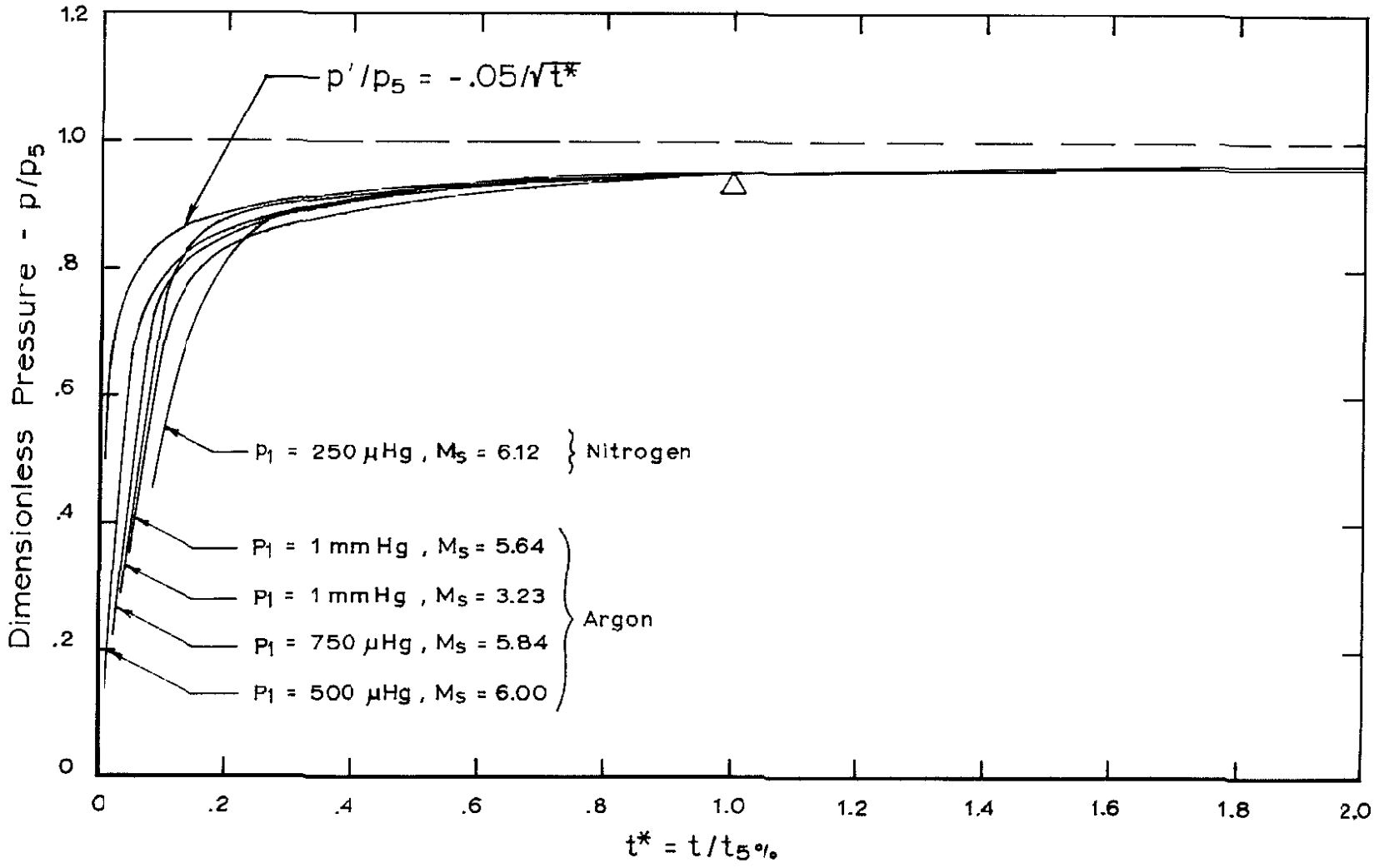

FIGURE 12 NON-DIMENSIONAL PLOT OF SEVERAL EXPERIMENTAL END WALL PRESSURE PROFILES

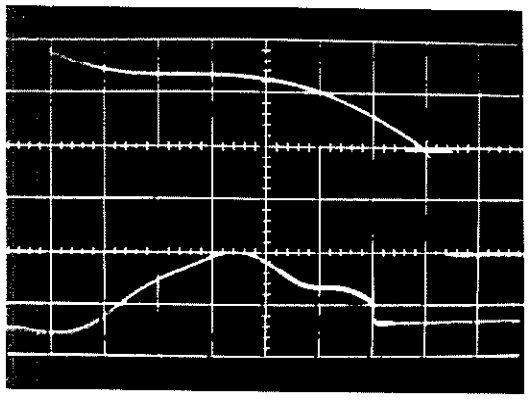

(a) $p_1 = 500\ \mu Hg$, $M_S = 6.42$

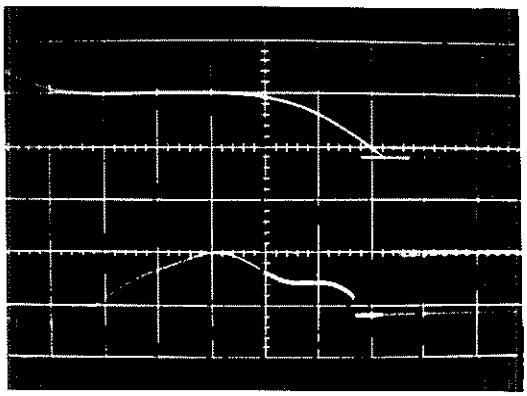

(b) $p_1 = 1\ mm Hg$, $M_S = 5.78$

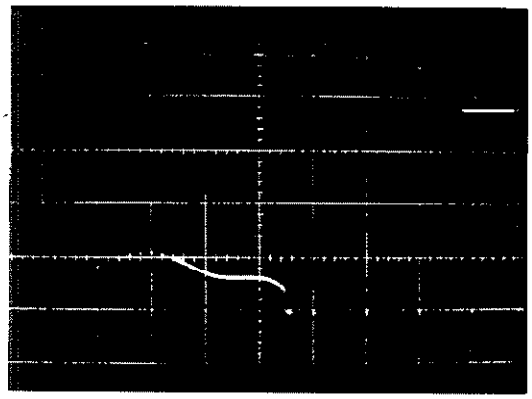

(c) $p_1 = 5\ mm Hg$, $M_S = 4.24$

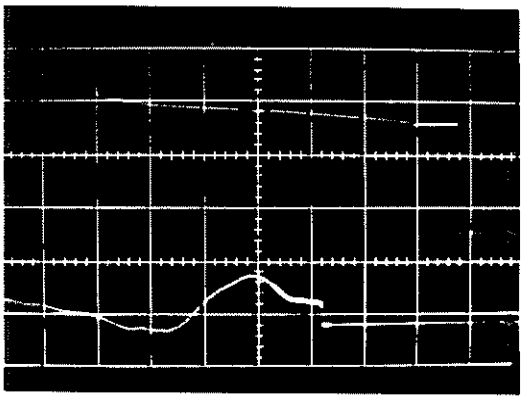

(d) $p_1 = 5\ mm Hg$, $M_S = 2.46$

Mark : Frozen-Frozen Jump

FIGURE 13 PRESSURE HISTORIES SHOWING THE EFFECT OF VIBRATIONAL RELAXATION IN CARBON DIOXIDE

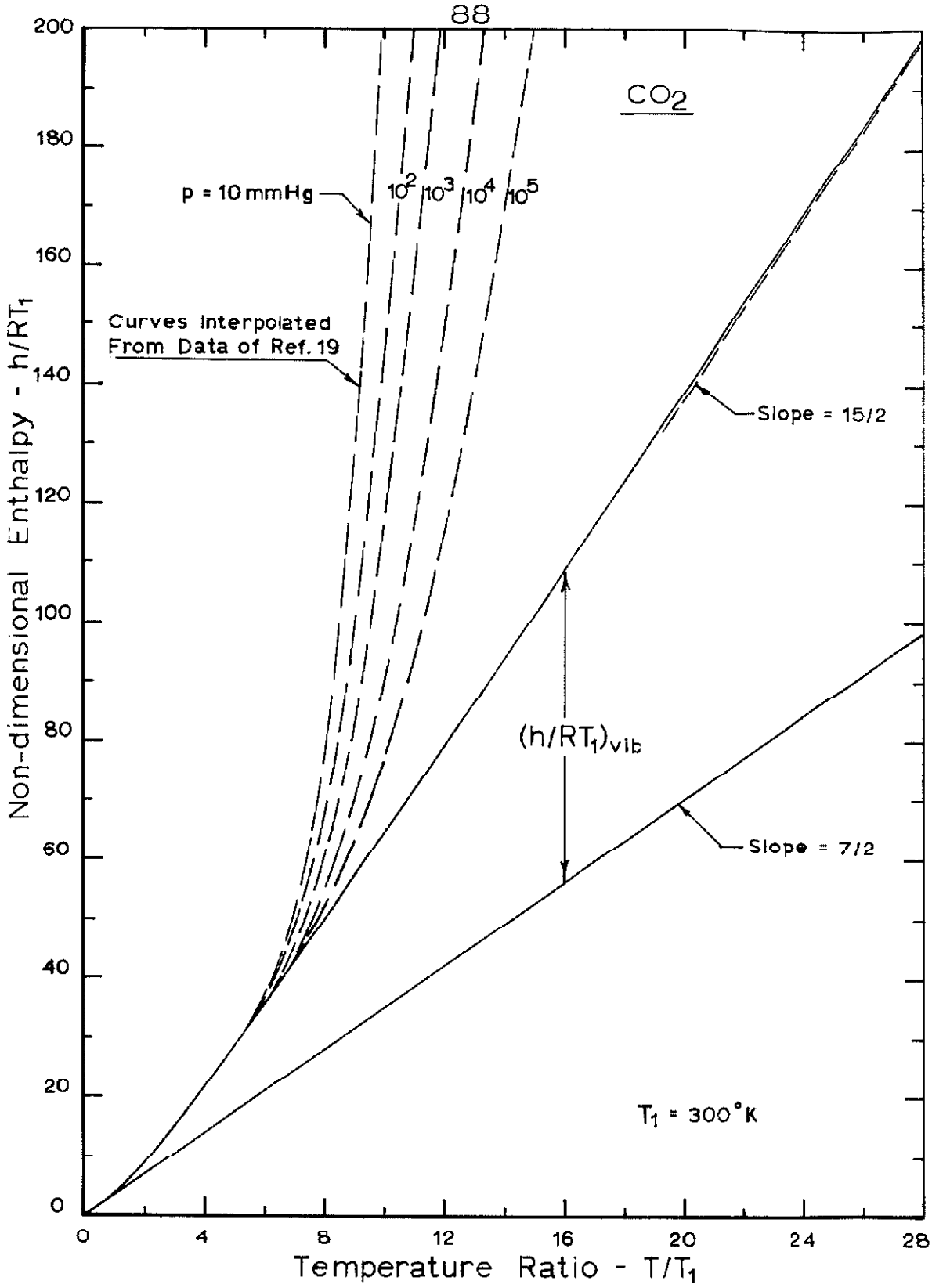

FIGURE 14 NON-DIMENSIONAL ENTHALPY h/RT_1 FOR CO_2

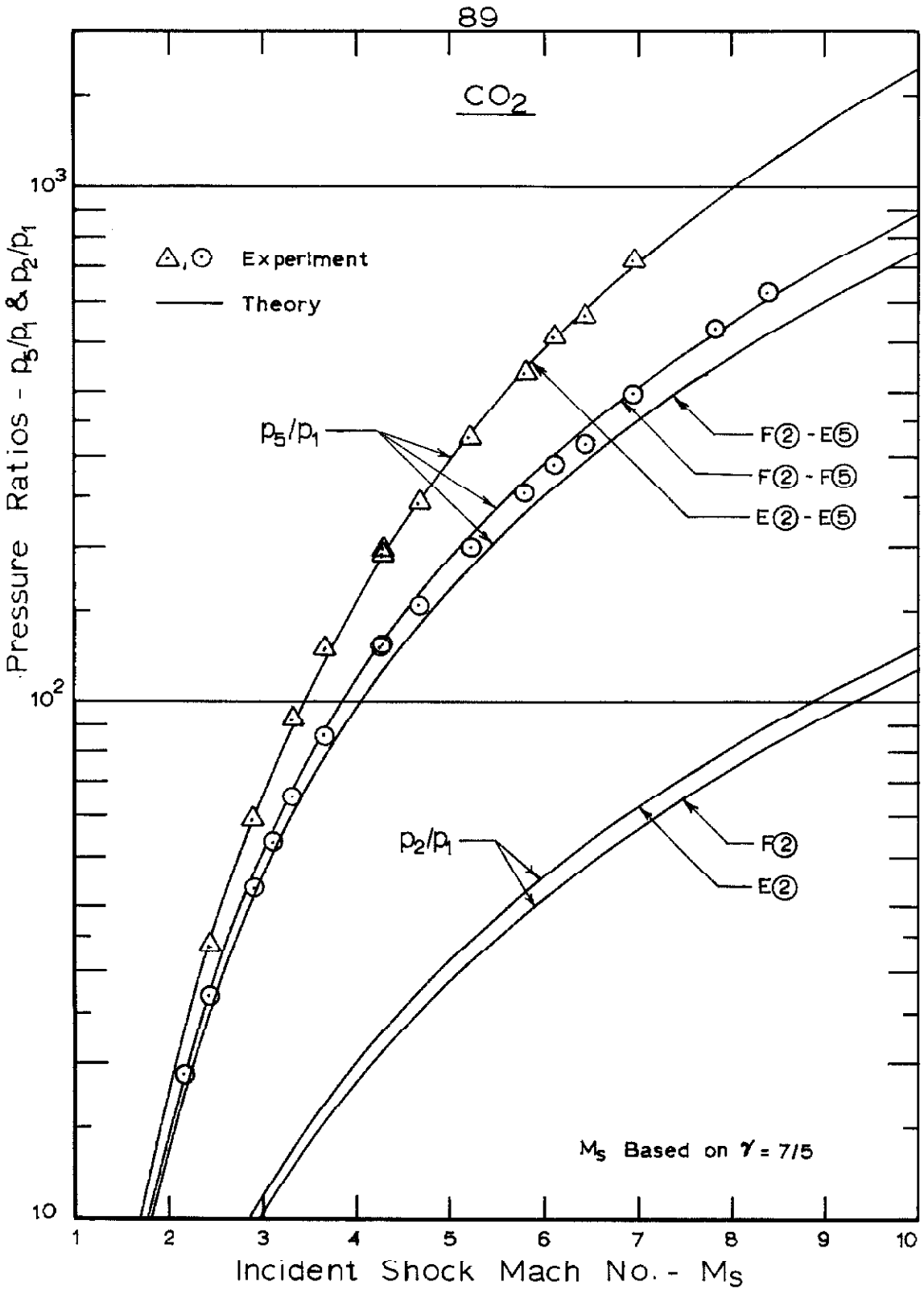

FIGURE 15 PRESSURE RATIOS ACROSS INCIDENT AND REFLECTED SHOCKS IN CO_2

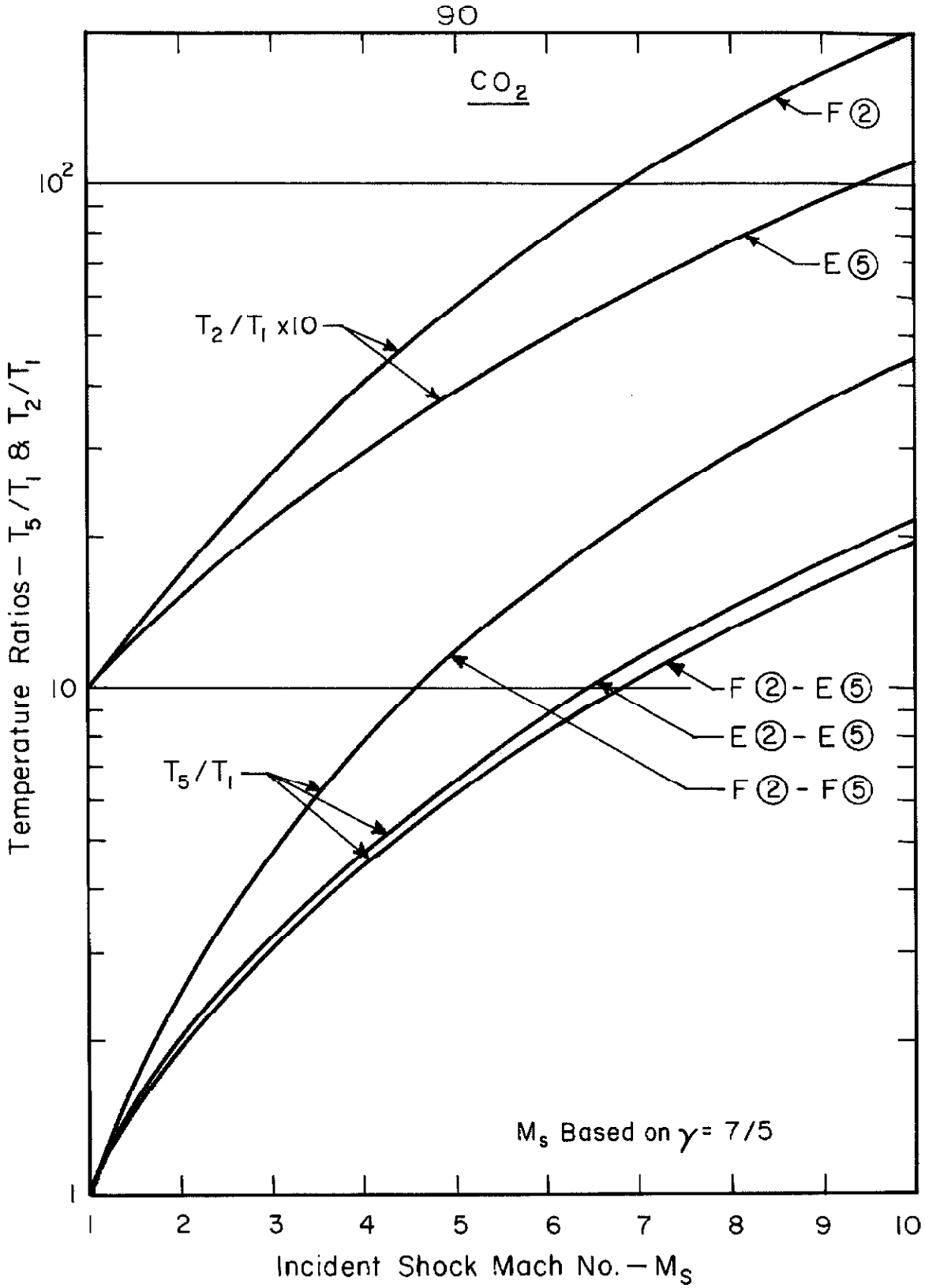

FIGURE 16 TEMPERATURE RATIOS ACROSS INCIDENT AND REFLECTED SHOCKS IN CO_2

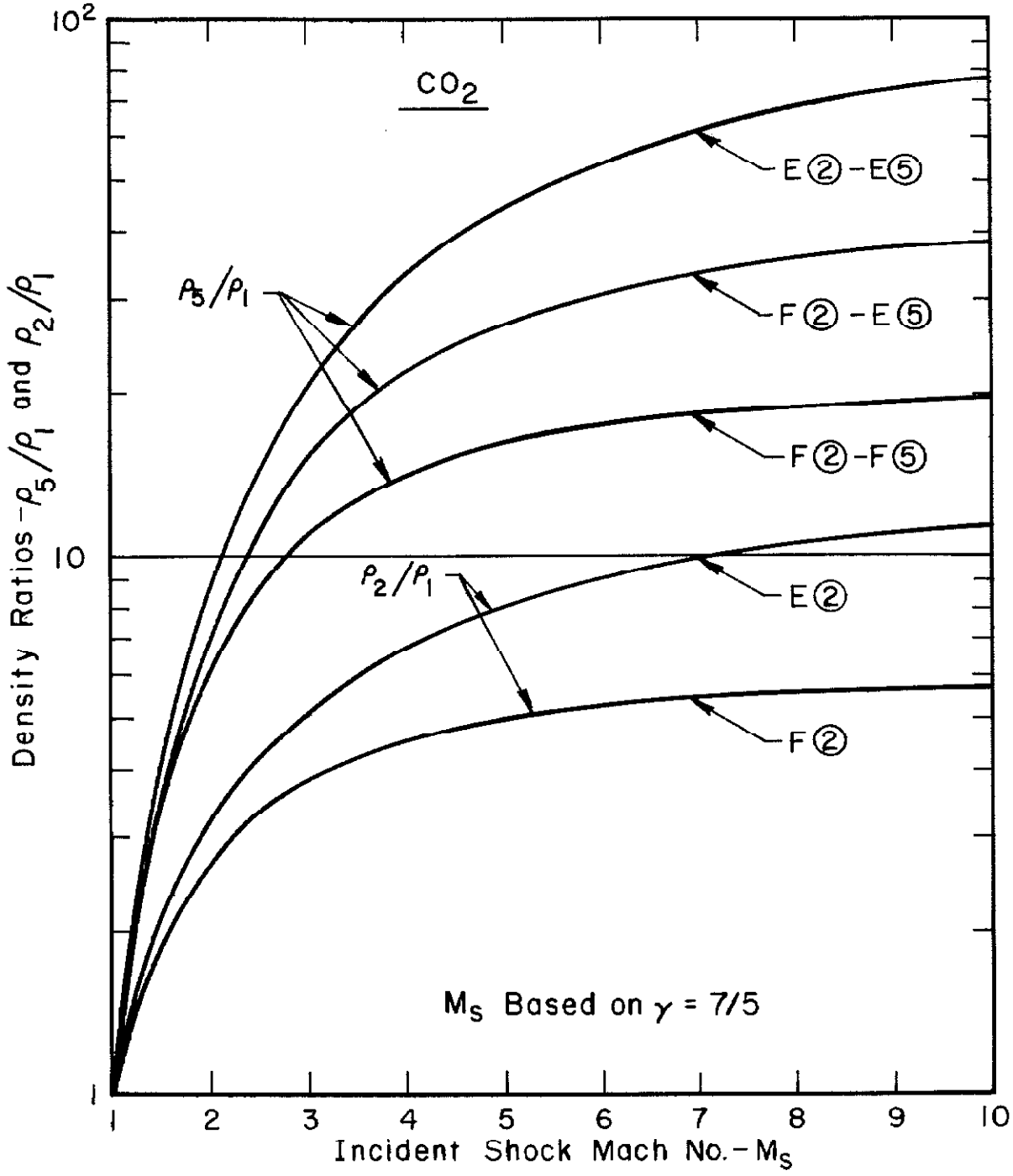

FIGURE 17 DENSITY RATIOS ACROSS INCIDENT AND REFLECTED SHOCKS IN CO_2

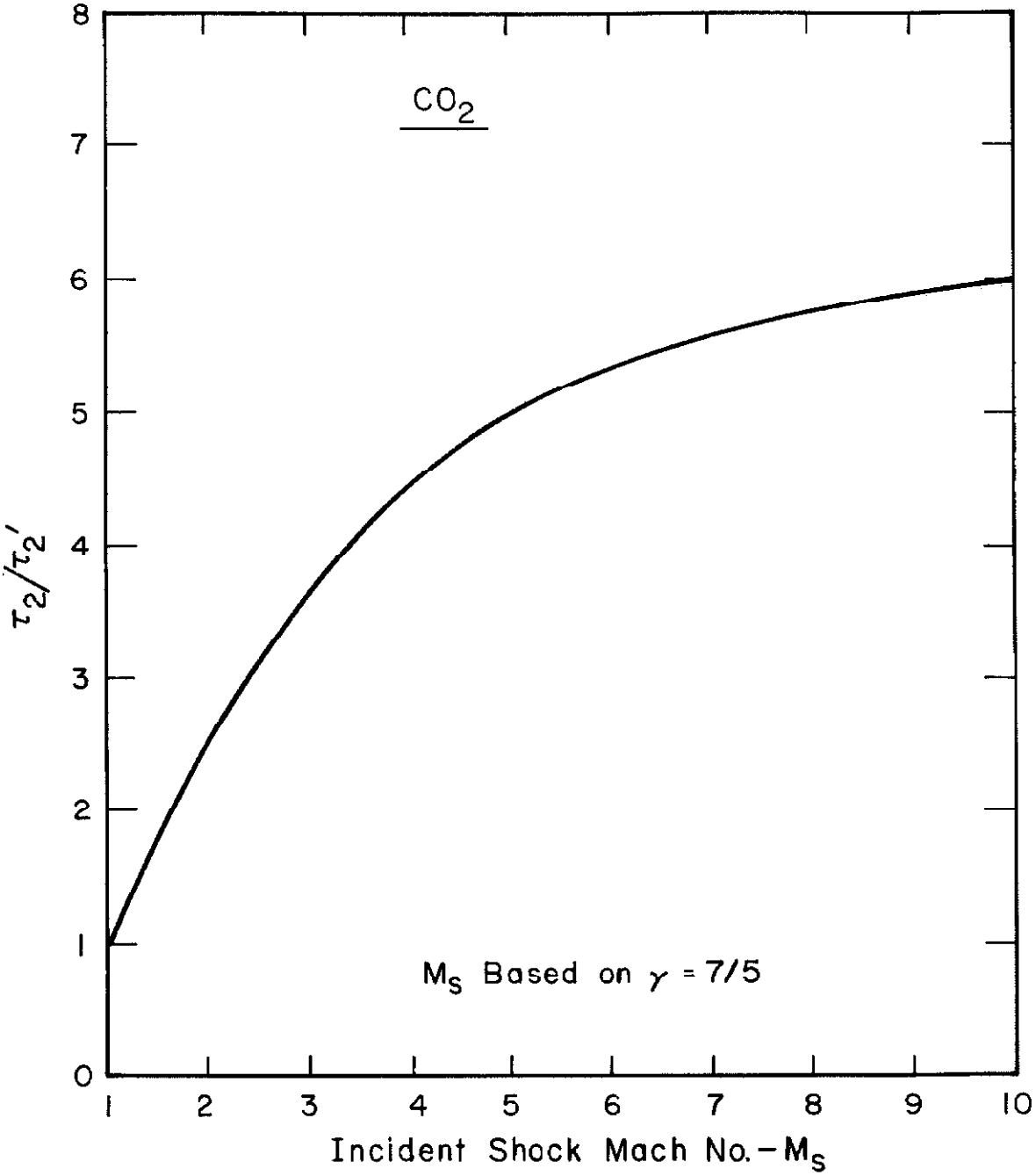

FIGURE 18 RATIO OF RELAXATION TIMES τ_2/τ_2' FOR A REFLECTED SHOCK IN CO_2

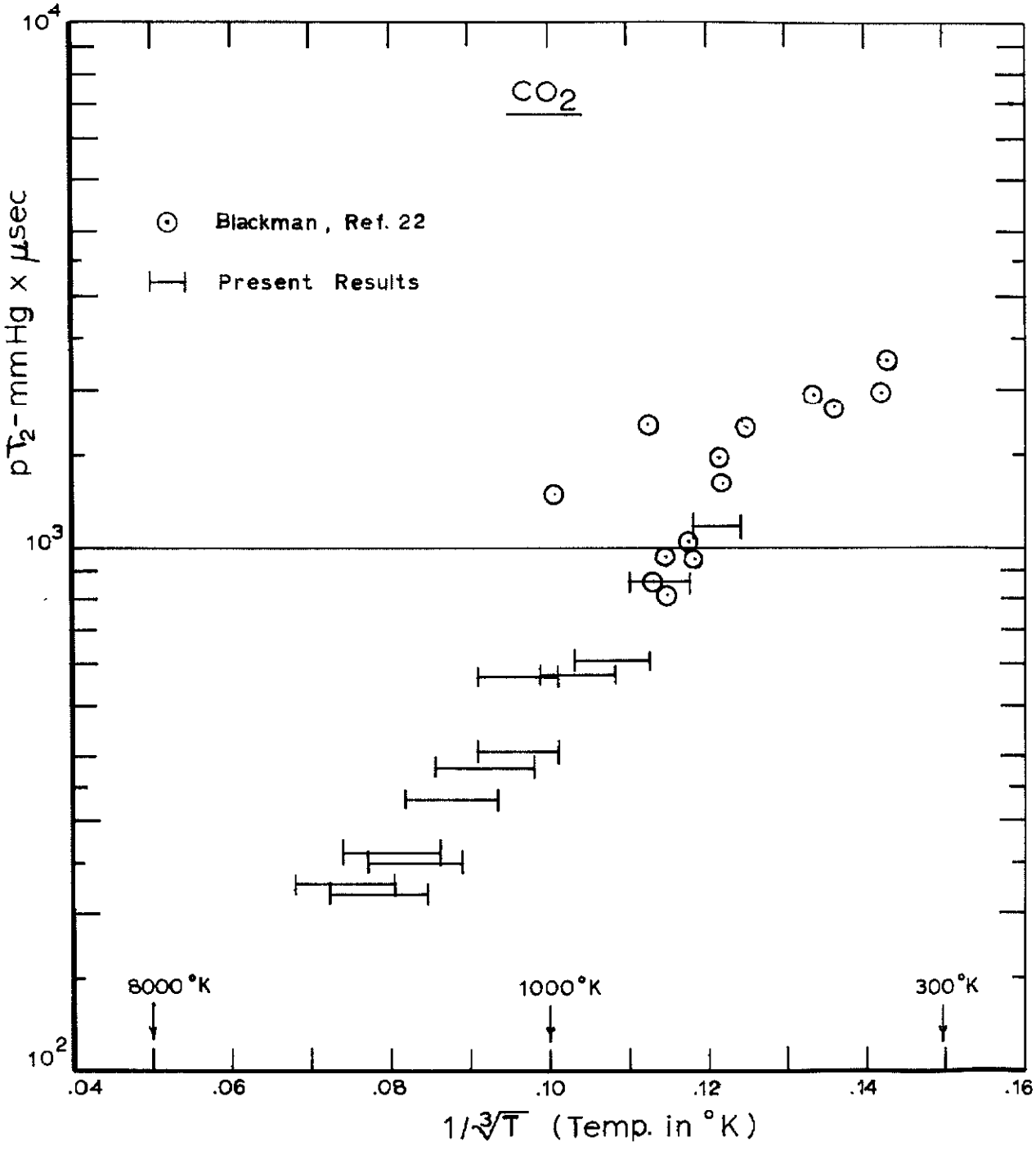

FIGURE 19 VIBRATIONAL RELAXATION TIME IN CO_2

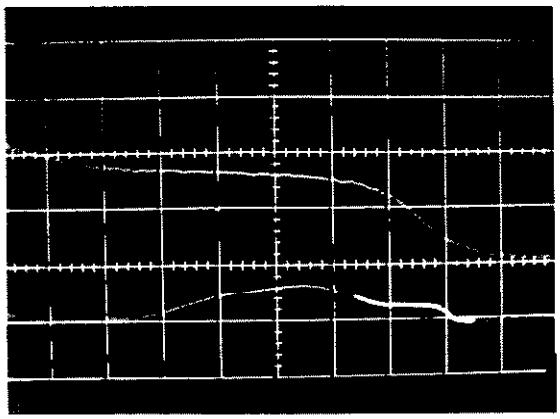

(a) $p_1 = 50\ \mu Hg$, $M_S = 7.32$

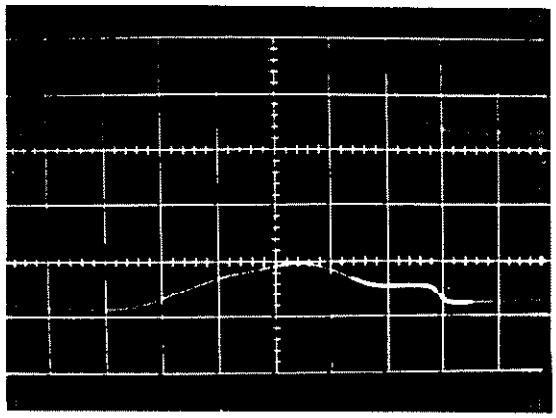

(b) $p_1 = 75\ \mu Hg$, $M_S = 7.08$

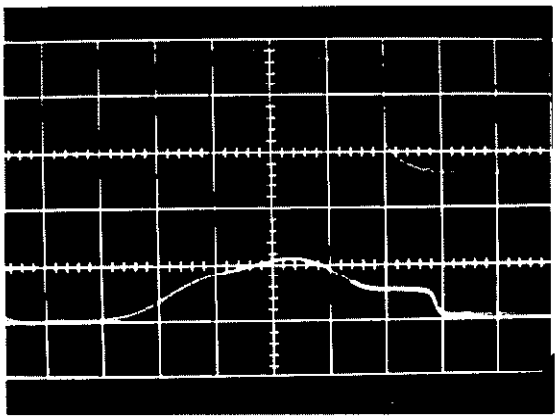

(c) $p_1 = 100\ \mu Hg$, $M_S = 6.85$

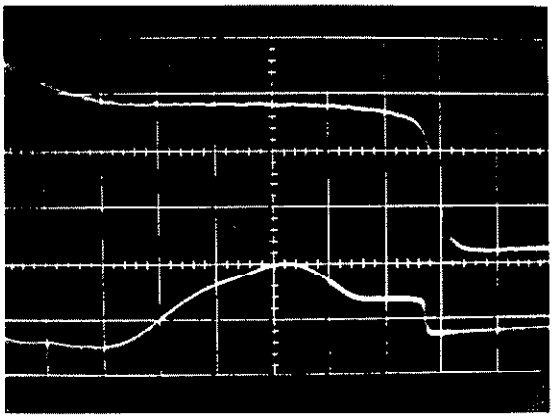

(d) $p_1 = 250\ \mu Hg$, $M_S = 6.35$

FIGURE 20 P_{xx} PROFILES FOR REFLECTED SHOCKS IN ARGON

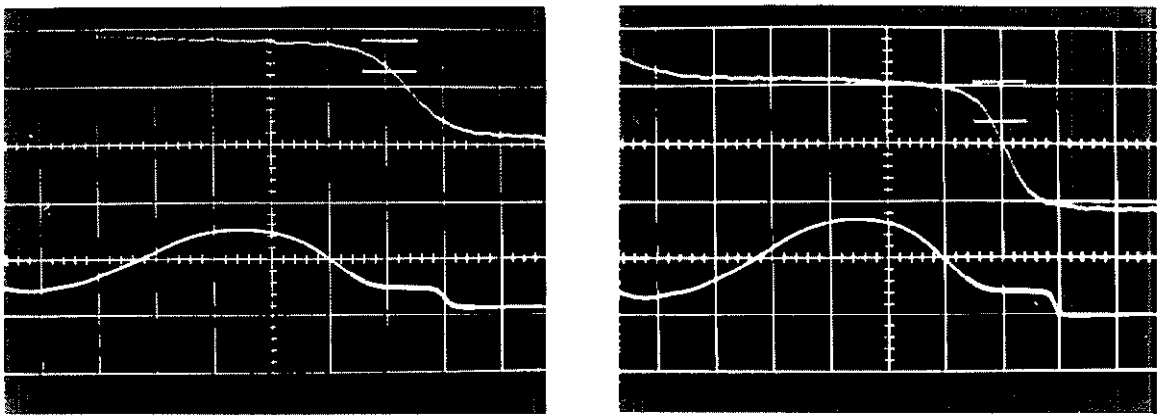

(a) $p_1 = 50\,\mu Hg$, $M_S = 6.41$

(b) $p_1 = 75\,\mu Hg$, $M_S = 6.30$

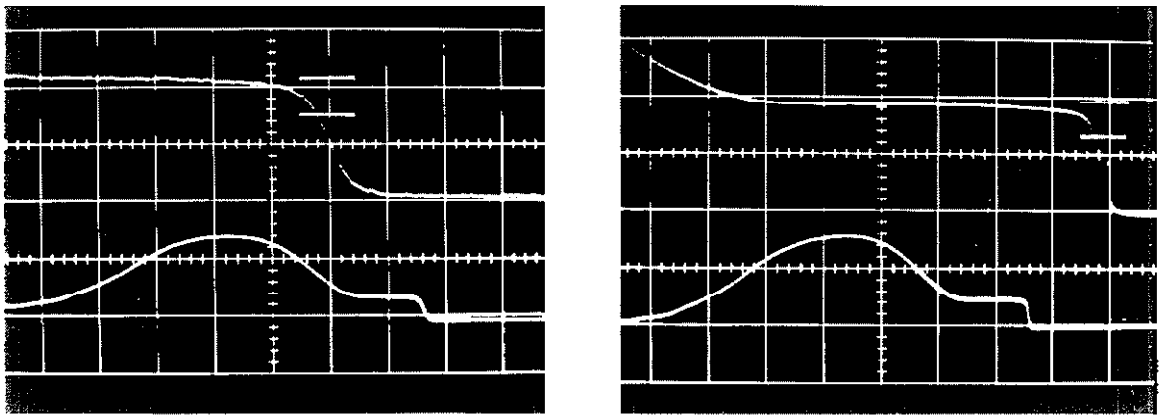

(c) $p_1 = 100\,\mu Hg$, $M_S = 5.55$

(d) $p_1 = 250\,\mu Hg$, $M_S = 5.61$

Upper Mark : $\gamma = 7/5$
Lower Mark : $\gamma = 5/3$

FIGURE 21 P_{xx} PROFILES FOR REFLECTED SHOCKS IN NITROGEN

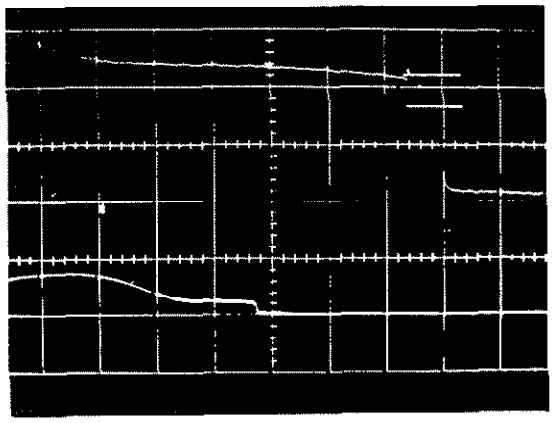

(a) $p_1 = 500\ \mu Hg$, $M_S = 3.45$

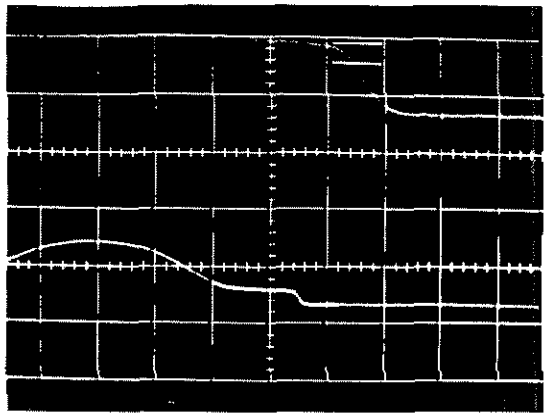

(b) $p_1 = 150\ \mu Hg$, $M_S = 3.76$

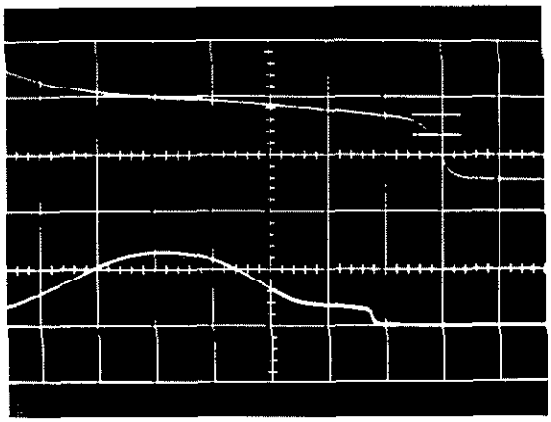

(c) $p_1 = 150\ \mu Hg$, $M_S = 5.36$

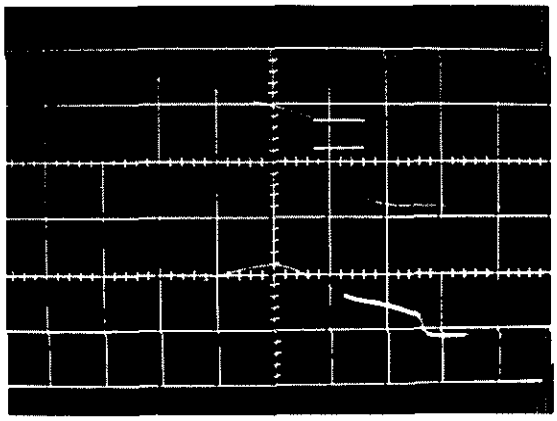

(d) $p_1 = 100\ \mu Hg$, $M_S = 7.80$

Upper Mark : $\gamma = 7/5$
Lower Mark : $\gamma = 5/3$

FIGURE 22 P_{xx} PROFILES FOR REFLECTED SHOCKS IN CARBON DIOXIDE

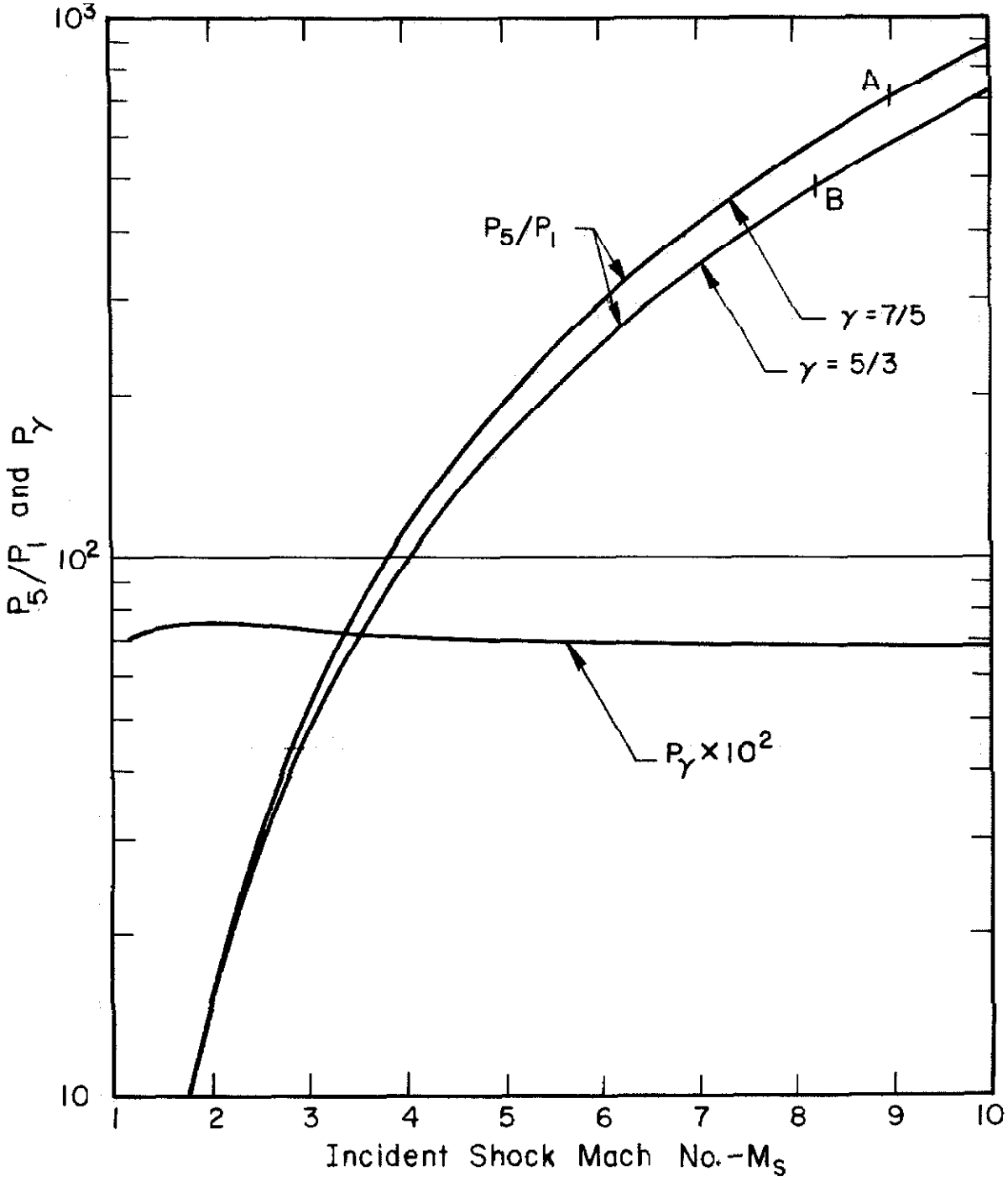

FIGURE 23 DIFFERENCE IN PRESSURE RATIO DUE TO ROTATIONAL RELAXATION

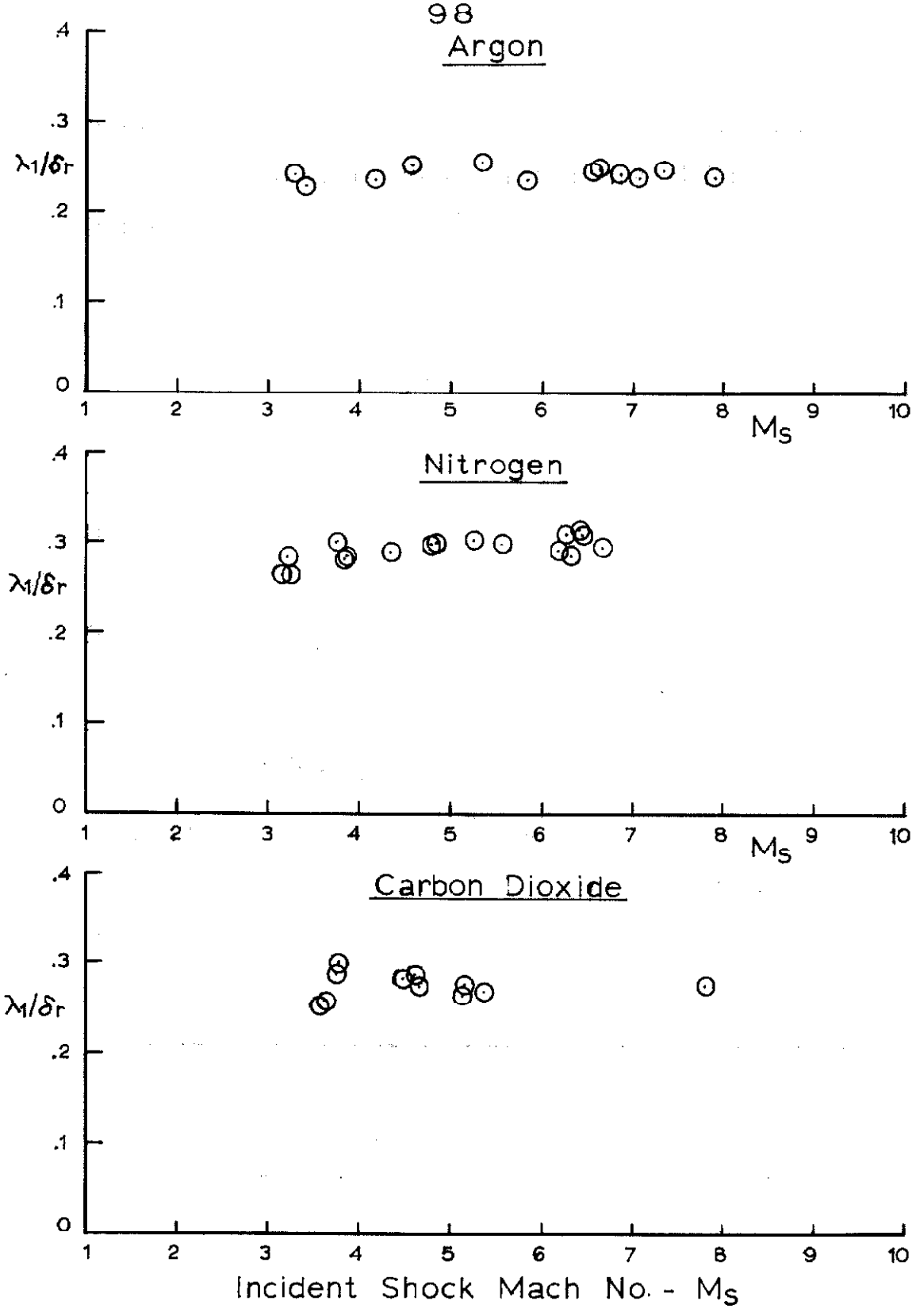

FIGURE 24 RECIPROCAL SHOCK THICKNESS FOR A REFLECTED SHOCK

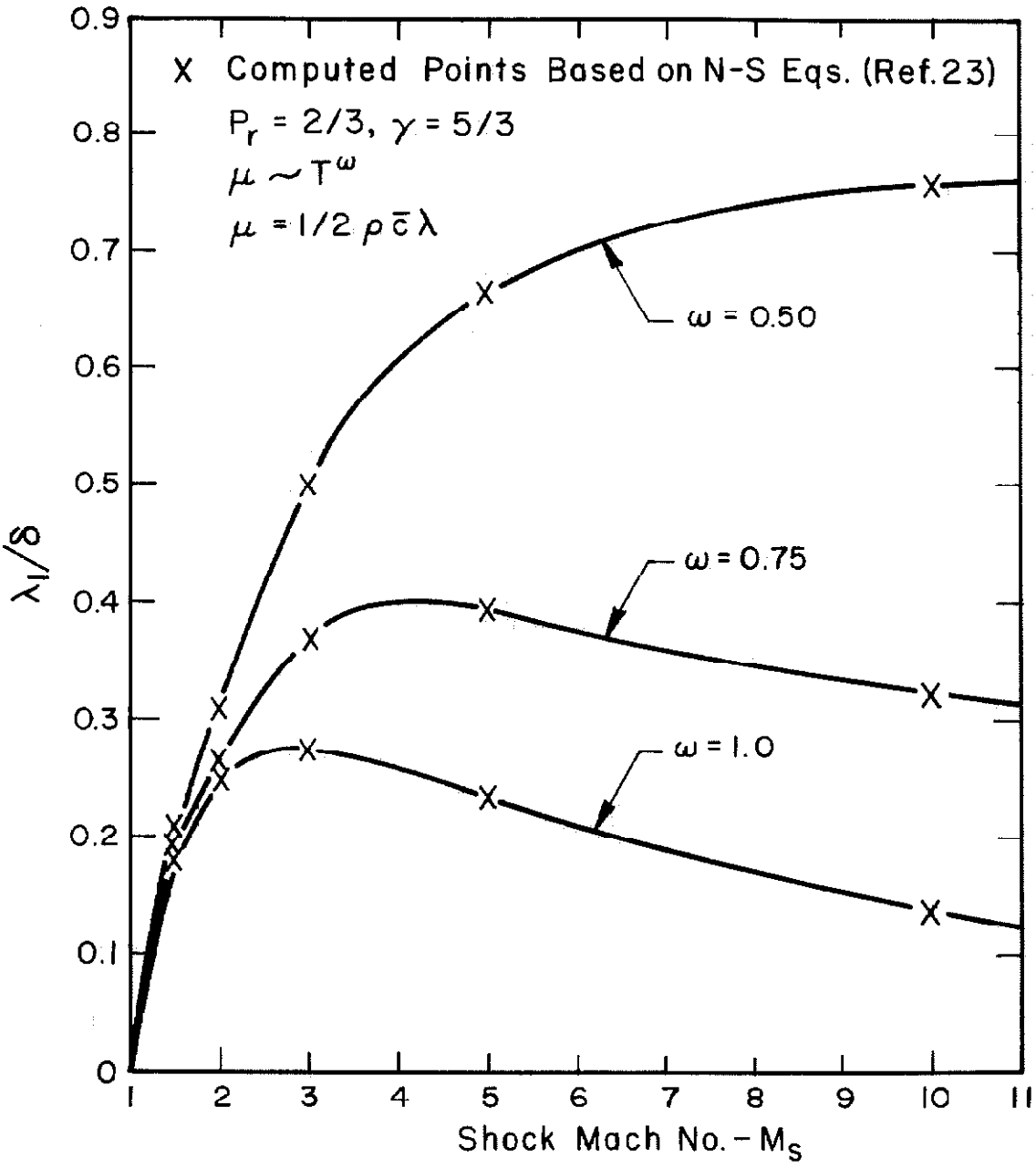

FIGURE 25 THEORETICAL RECIPROCAL SHOCK THICKNESS FOR A FREE RUNNING SHOCK

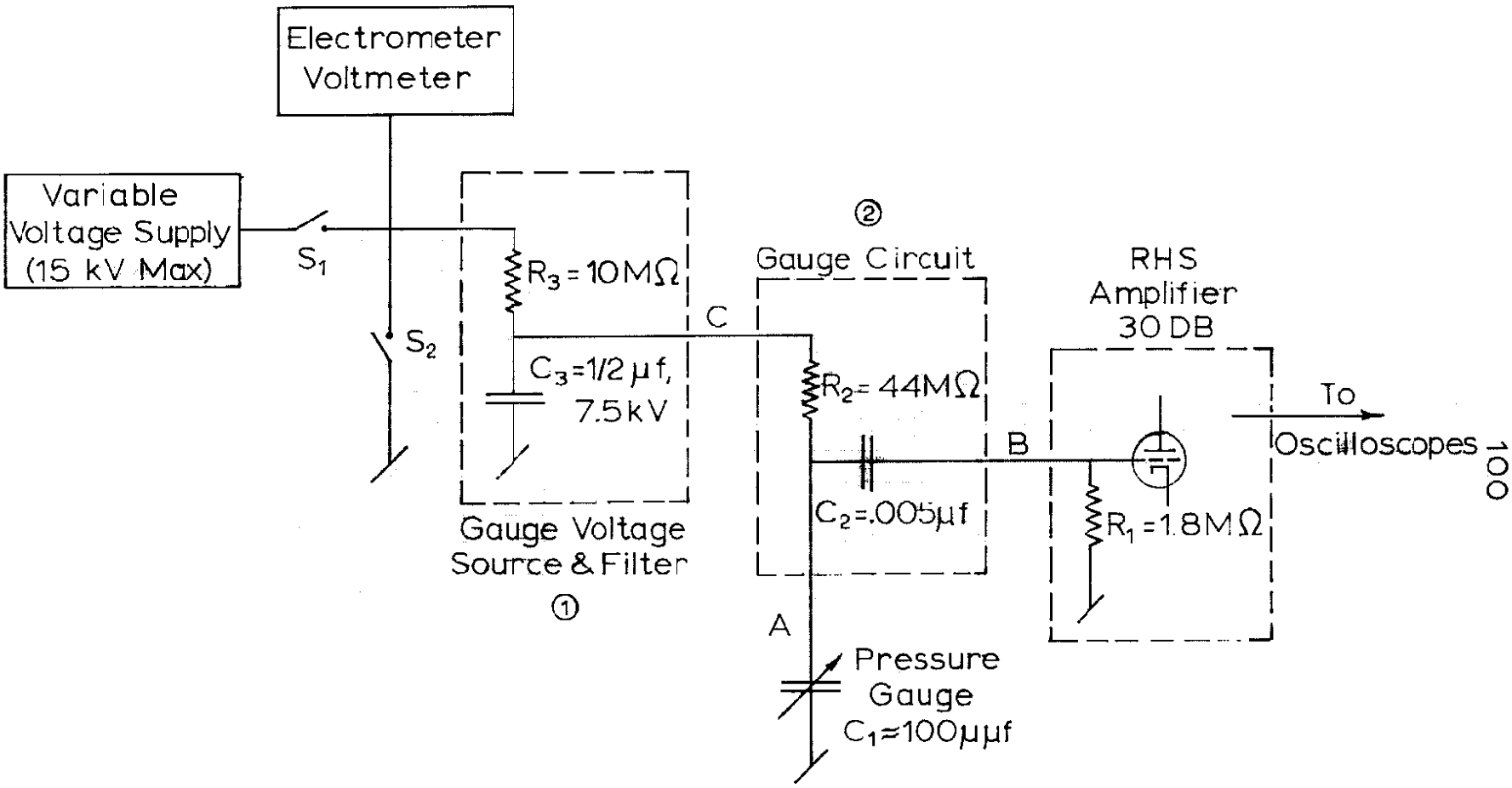

FIGURE 26 DETAILS OF PRESSURE GAUGE CIRCUIT

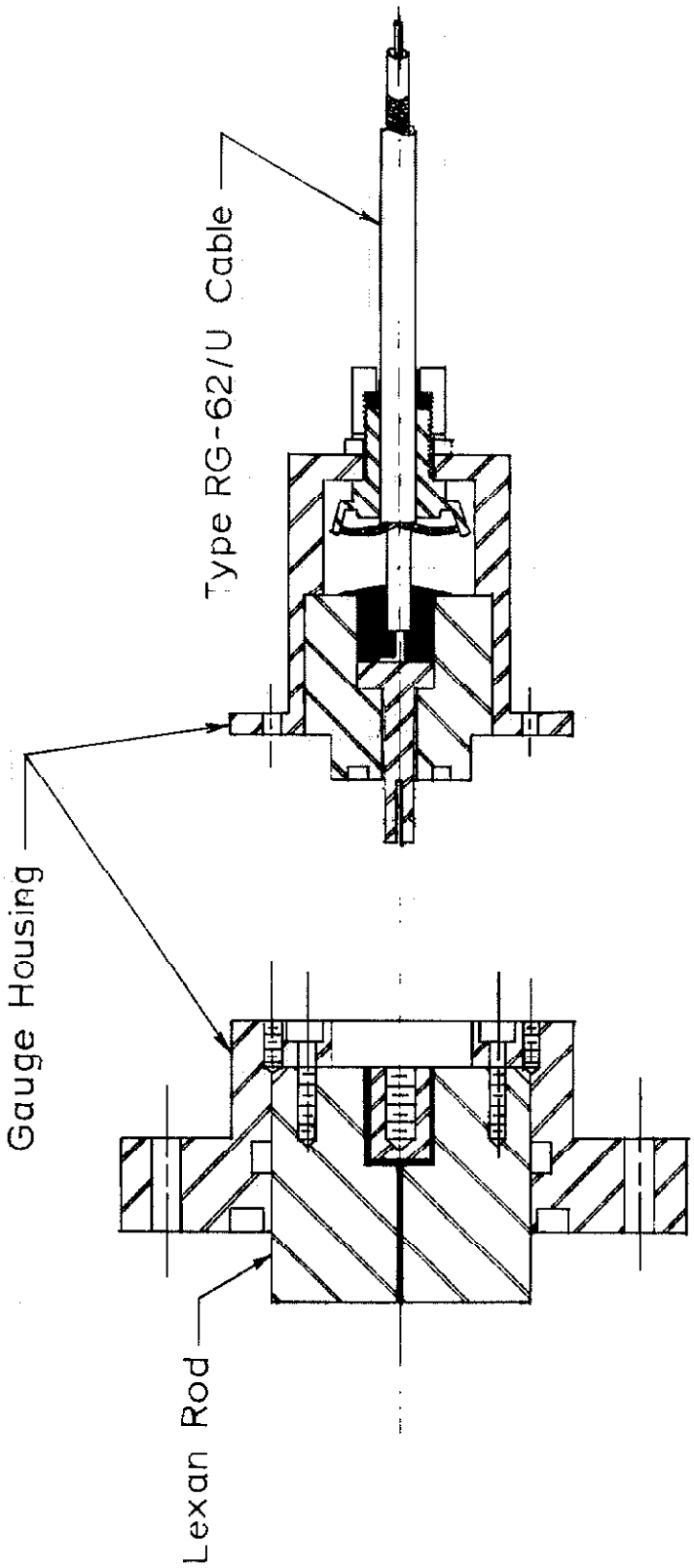

FIGURE 27 DRAWING OF PRESSURE GAUGE ASSEMBLY AND HIGH VOLTAGE CONNECTION

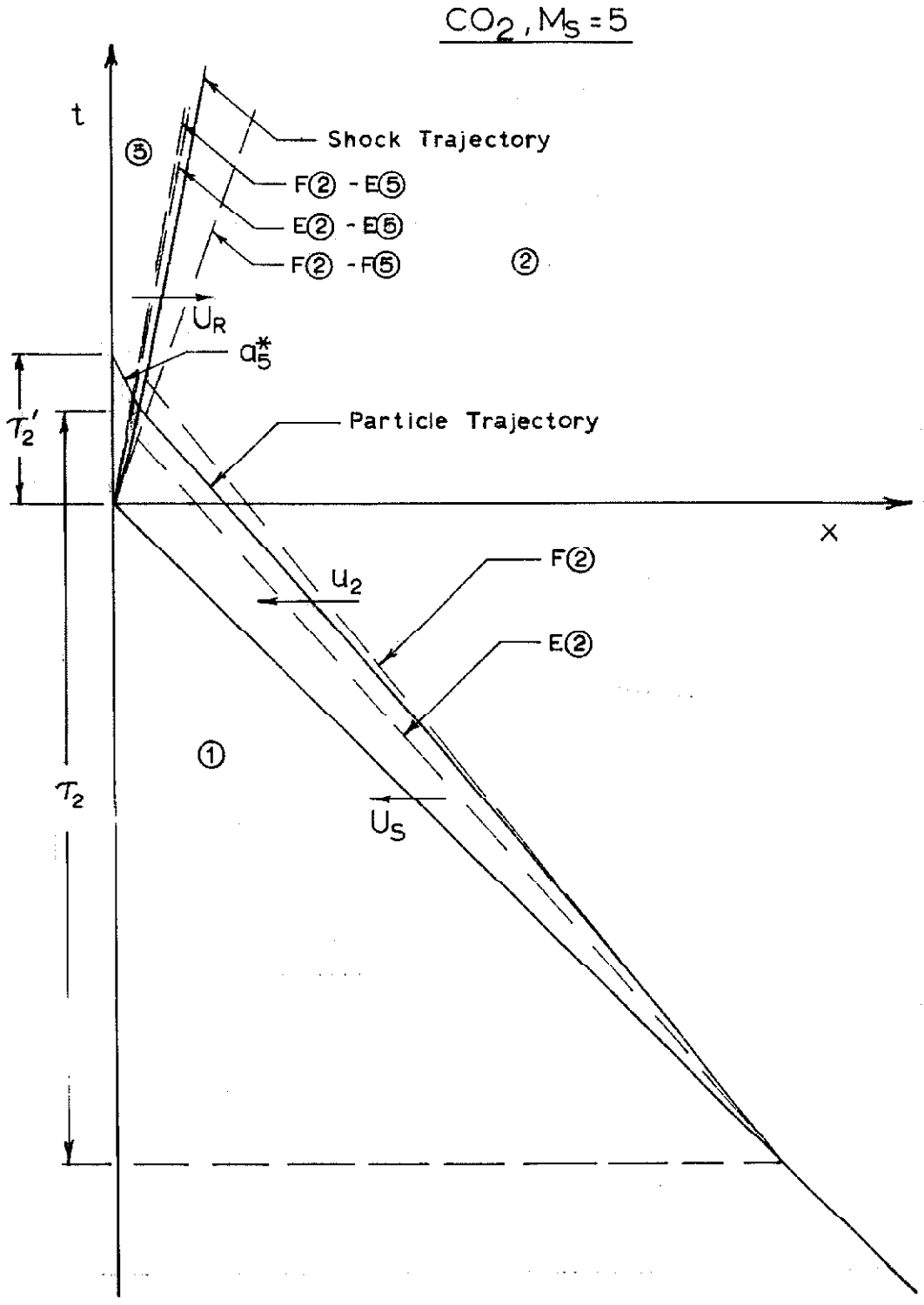

FIGURE 28 SCALE DRAWING OF x-t DIAGRAM FOR A REFLECTED SHOCK IN CO_2 AND $M_S = 5$

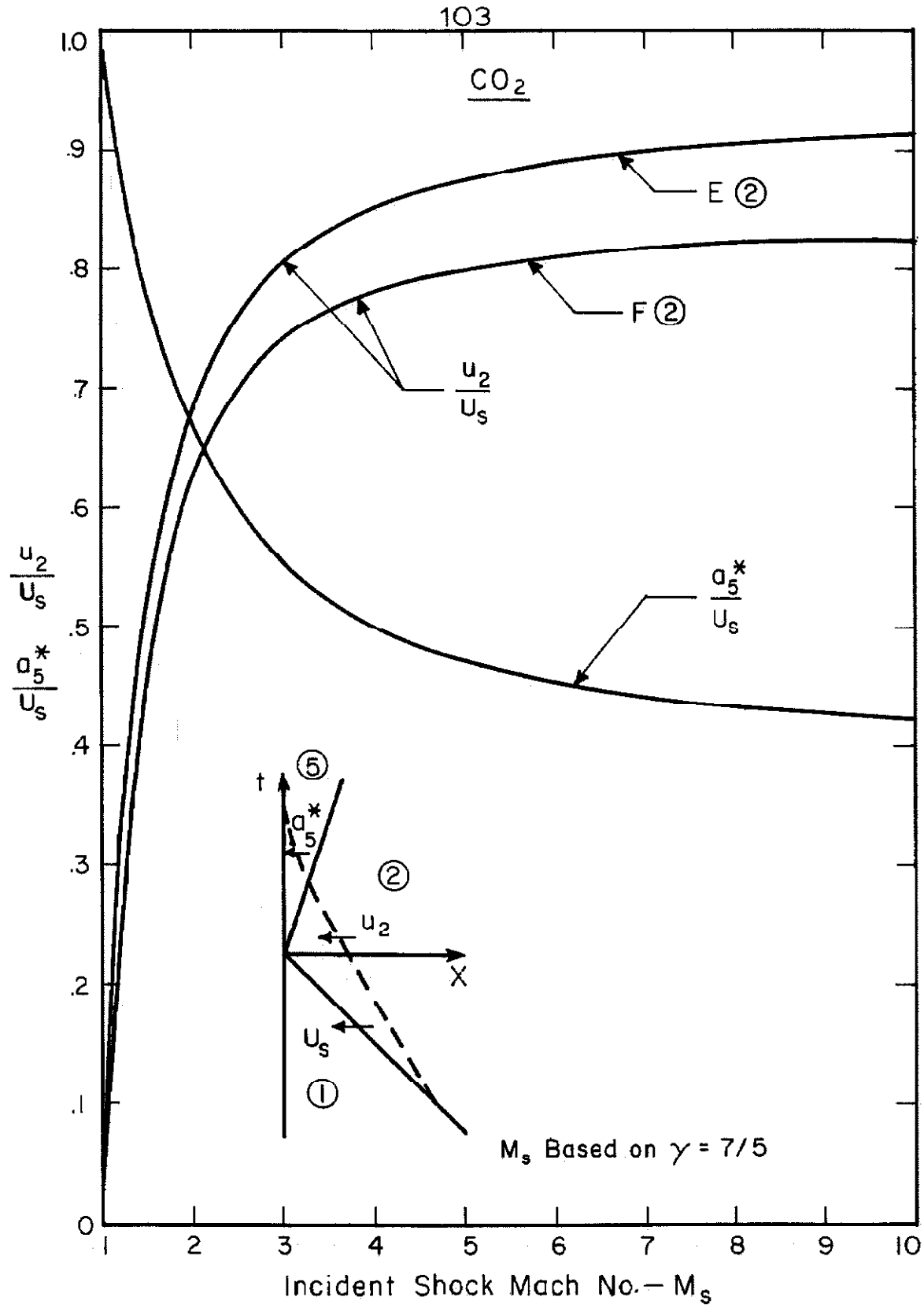

FIGURE 29. VELOCITY RATIOS u_2/U_s AND a_5^*/U_s FOR A REFLECTED SHOCK IN CO_2

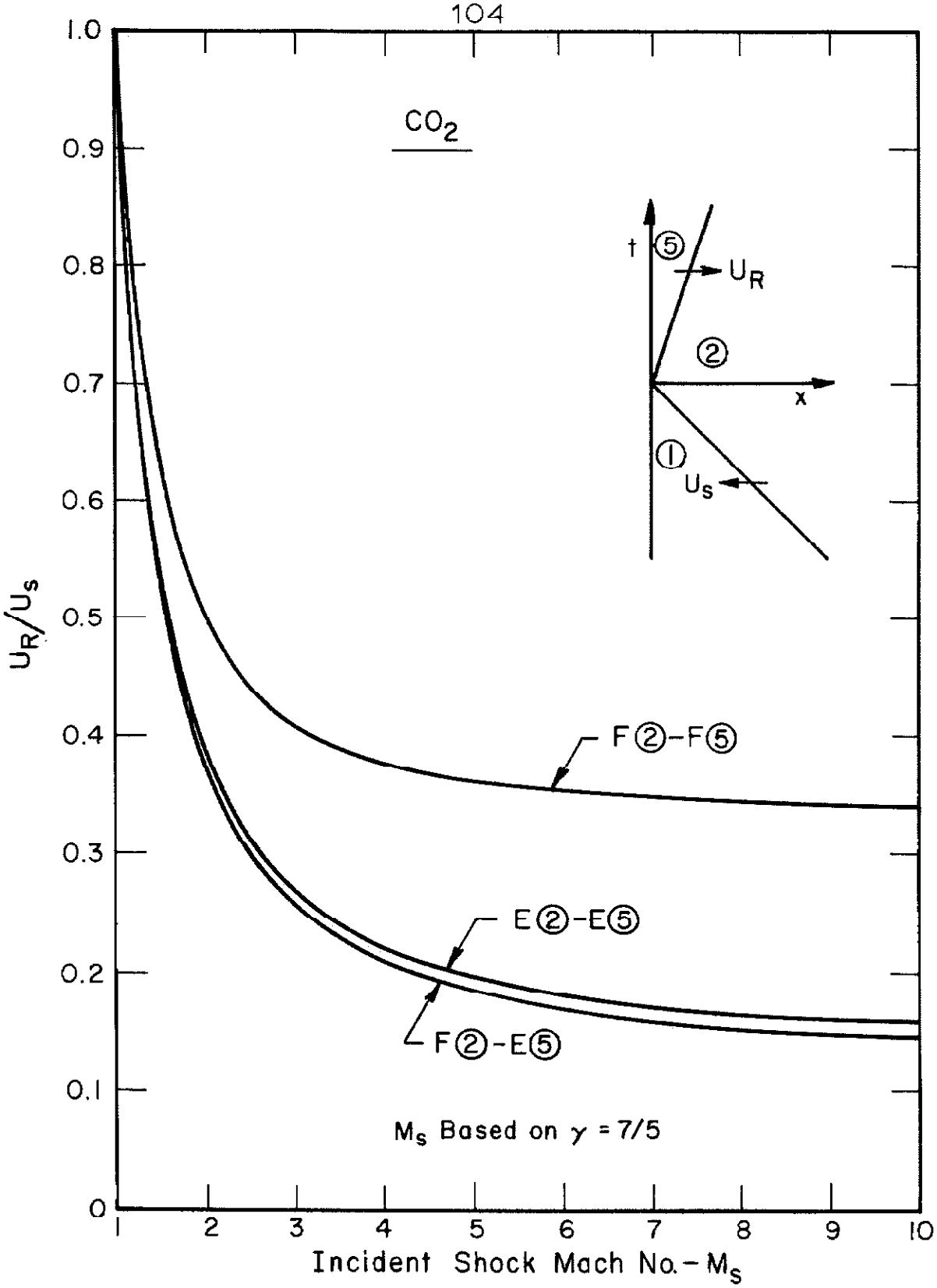

FIGURE 30 RATIO OF REFLECTED SHOCK SPEED TO INCIDENT SHOCK SPEED FOR CO_2